https://ntrs.nasa.gov/search.jsp?R=20110022489 2018-07-21T09:13:53+00:00Z

Solar Dynamics Observatory On-orbit Jitter Testing, Analysis, and Mitigation Plans

Kuo-Chia (Alice) Liu[1]
NASA Goddard Space Flight Center, Greenbelt, MD, 20771

Carl A. Blaurock[2]
Nightsky Systems Inc., Raleigh, NC , 27601

Kristin L. Bourkland[3], Wendy M. Morgenstern[4], and Peiman G. Maghami[5]
NASA Goddard Space Flight Center, Greenbelt, MD, 20771

The recently launched Solar Dynamics Observatory (SDO) has two science instruments onboard that required sub-arcsecond pointing stability. Significant effort has been spent pre-launch to characterize the disturbances sources and validating jitter level at the component, sub-assembly, and spacecraft levels. However, an end-to-end jitter test emulating the flight condition was not performed on the ground due to cost and risk concerns. As a result, the true jitter level experienced on orbit remained uncertain prior to launch. Based on the pre-launch analysis, several operational constraints were placed on the observatory aimed to minimize the instrument jitter levels. If the actual jitter is below the analysis predictions, these operational constraints can be relaxed to reduce the burden of the flight operations team. The SDO team designed a three-day jitter test, utilizing the instrument sensors to measure pointing jitter up to 256 Hz. The test results were compared to pre-launch analysis predictions, used to determine which operational constraints can be relaxed, and analyzed for setting the jitter mitigation strategies for future SDO operations.

Nomenclature

dt	=	simulation sample time
G_{ATF}	=	instrument stabilization system attenuation transfer function
h	=	wheel momentum vector
h_{bias}	=	wheel momentum bias
K_g	=	momentum redistribution control gain
M_1	=	initial index of sliding window
M_2	=	end index of sliding window
N	=	number of sampled data points in a sliding window with width τ
σ_j	=	root-mean-square jitter
S_{zz}	=	power spectral density of LOS motion
τ	=	instrument exposure time
θ	=	LOS motion
V_n	=	null space vector
ω	=	frequency in Hz

[1]Aerospace Engineer, Attitude Control System Engineering Branch, Greenbelt MD, 20771, AIAA Lifetime Member.
[2]President, Nightsky Systems Inc., 301 Fayetteville St, Raleigh NC 27601, AIAA Member.
[3]Aerospace Engineer, Attitude Control System Engineering Branch, Greenbelt MD, 20771.
[4]Aerospace Engineer, Attitude Control System Engineering Branch, Greenbelt MD, 20771, AIAA Member.
[5]Aerospace Engineer, Attitude Control System Engineering Branch, Greenbelt MD, 20771, AIAA Member.

I. Introduction

THE Solar Dynamics Observatory (SDO) was designed to understand the Sun and the Sun's influence on Earth. SDO was launched on February 11, 2010 carrying three scientific instruments: the Atmospheric Imaging Assembly (AIA), the Helioseismic and Magnetic Imager (HMI), and the Extreme Ultraviolet Variability Experiment (EVE). Both AIA and HMI are sensitive to high frequency pointing perturbations and have sub-arcsecond level line-of-sight (LOS) jitter requirements. Extensive modeling and analysis efforts were directed in estimating the amount of jitter disturbing the science instruments. In order to verify the disturbance models and validate the jitter performance prior to launch, many jitter-critical components and subassemblies were tested either by the mechanism vendors or at the NASA Goddard Space Flight Center (GSFC)[1].

Although detailed analysis and assembly level tests were performed to obtain good jitter predictions, there were still several sources of uncertainties in the system. The structural finite element model did not have all the modes correlated to test data at high frequencies (>50 Hz). The performance of the instrument stabilization system was not known exactly but was expected to be close to the analytical model. A true disturbance-to-LOS observatory level test was not available due to the tight schedule of the flight spacecraft, the cost in time and manpower, difficulties in creating gravity negation systems, and risks of damaging flight hardware. In order to protect the observatory jitter performance against model uncertainties, the SDO jitter team devised several on-orbit jitter reduction plans in addition to reserve margins on analysis results. Since some of these plans severely restricted the capabilities of several spacecraft components (e.g. wheels and high gain antennas), the SDO team performed on-orbit jitter tests to determine which jitter reduction plans, if any, were necessary to satisfy science LOS jitter requirements. The SDO on-orbit jitter tests were designed to satisfy the following four objectives:

1. Determine the acceptable reaction wheel operational speed range during Science Mode.
2. Determine high gain antenna (HGA) algorithm jitter parameters (number of stagger steps and enable/disable no-step-requests).
3. Determine acceptable EVE instrument filter wheel spin rates.
4. Determine if the AIA instrument mechanism generates acceptable self-induced jitter and if the AIA observation sequence needs to be modified to reduce or minimize the effects of the AIA filter wheels.

The on-orbit jitter tests could be performed on SDO mainly because the AIA and HMI instruments contain sensors that also acted as jitter sensors. The primary jitter sensor for all the jitter test was the HMI limb sensor measuring LOS errors at 512 Hz. The four AIA guide telescope signals were also available with sample rates of 256 Hz for telescopes #1 and #3, and 128 Hz for telescopes #2 and #4. Both HMI and AIA instruments can store 3 minutes of data and require 30 minutes to download the data to the ground. The data downlink time is about a factor of ten times the data storage time. The data storage and download time constraints drove the design of some of the jitter tests.

This paper first provides a brief description of the integrated dynamic model used for all pre-launch jitter analysis in Section II. The detailed information on the pre-launch analysis, on-orbit jitter test plan, comparison of jitter measurements to predictions, and final jitter mitigation plan executed on SDO are presented in Sections III through VI for each of the four jitter tests. On-orbit test results summary and important lessons learned are provided in Section VII of this paper.

II. Integrated Modeling and Analysis

The SDO jitter performance is defined as the LOS motion measured at the instrument detectors. The spacecraft attitude control system (ACS) is capable of removing large, slowly varying LOS errors that fall within the bandwidth (~0.05 Hz) of the pointing controller. Both AIA and HMI have additional instrument stabilization systems (ISS) to reduce mid-frequency range LOS disturbances (up to 20-40 Hz). The residual LOS motion, after ACS and ISS compensation, measured on the instrument detectors must be less than 170 milli-arcsecond (masec), 1-σ for AIA and 140 masec, 1- σ for HMI.

The SDO jitter analysis employs an integrated modeling approach where disturbance, structures, controls, and performance metrics are combined into one dynamic model to predict the end-to-end LOS performance of the system. The disturbance models are inputs to the system, the structural dynamic model is created from the finite element analysis, the ACS model stabilizes the rigid body modes of the structural model, the optical model maps all the optical motions to the LOS motion, and the instrument stabilization system (ISS) models the LOS motion attenuation from the instrument controllers. The outputs from the integrated model are the LOS motion measured at the AIA and HMI detectors. In this section, more details on the structure and control models, and performance metric computations are provided. Each disturbance source model is described in the pre-test analysis section below.

A. Structural and Damping Models

The SDO structural dynamics model was created using the Finite Element method. The model consists of a spacecraft bus model, propulsion module, instrument module, and secondary structure created by GSFC, and an Instrument Optical Package (AIA and HMI models) provided by Lockheed Martin and Laboratory for Atmospheric and Space Physics. Loral provided a detailed HGA model. The models were integrated by GSFC. The spacecraft bus model was augmented with four copies of a four-node representation of the stepper motor and gearbox, developed by Nightsky Systems, that correctly represents the unpowered stiffness of the actuator, and provides the correct inputs for the electromagnetic motor torques[2]. The normal modes analysis run was performed using MSC/NASTRAN and produced over 650 modes between 0 and 200 Hz.

The damping model assumed uncoupled modal damping. The scalar damping value, used for all modes, was calibrated by test[1]. The test article comprised the Structural Verification Unit bus, the flight Instrument Module, three AIA mass simulators and one AIA dynamic simulator, and an HMI mass simulator. The test article was mounted on air bags to give flight-like boundary conditions and was excited using a proof mass actuator through a force-gage-equipped stinger. Tests at several forcing levels (at least two, three if noise level permitted) provided amplitude dependence information. Frequency Response Functions (FRFs) from input force to 19 accelerometer responses were acquired with a DataMax data acquisition system. The FRFs were fit with state space models using system identification methods, and the damping was extracted from the models. The results showed that 0.3% is a reasonably conservative damping ratio to be used for pre-launch jitter analysis; there is a 90% probability that damping for any mode will be at or above this value.

B. Control Models

SDO features two control systems that influence the pointing of the spacecraft: (1) ACS and (2) ISS. The ACS uses reaction wheels to stabilize rigid body pointing of the observatory. The ACS control system design, the wheel torque models, and the sensor models are provided by the SDO ACS analysis team. The attitude controller consists of a standard proportional-integral-derivative (PID) controller and a second-order structural filter for suppressing low frequency flexible modes and gain stabilizing the system. For jitter analysis, the main purpose of the ACS is to stabilize the three rigid-body modes. The ACS has no impact on the high frequency behavior or jitter motion of the closed-loop system.

Both AIA and HMI have an ISS that further attenuates residual pointing errors around body Y and Z axes (or tip/tilt of the LOS vector) from the ACS. See Figure 1 for coordinate system definition. The ISS has a much higher bandwidth than the ACS and does impact the jitter performance of the system. These controllers are designed and constructed by engineers at Lockheed Martin. Each AIA science telescope is accompanied by a guide telescope (GT) that uses limb sensors to provide pointing jitter signals to the ISS for image motion correction. The AIA ISS employs a Piezoelectric Transducer (PZT) actuated tip/tilt secondary mirror located inside the science telescope to center the image on the detector. Since the actuated mirror is not in the detection (optical) path of the limb sensor, the AIA has an open-loop ISS design. The performance of the AIA ISS depends on the calibration of the GT error signal and the image motion introduced by the PZT actuator. HMI also has limb sensors to feed back error signals to its ISS which drives a tip/tilt mirror to reduce image motion. Unlike the AIA design, the actuated mirror for HMI is in the optical path of the limb sensor. Therefore, the HMI ISS system operates in a closed-loop mode.

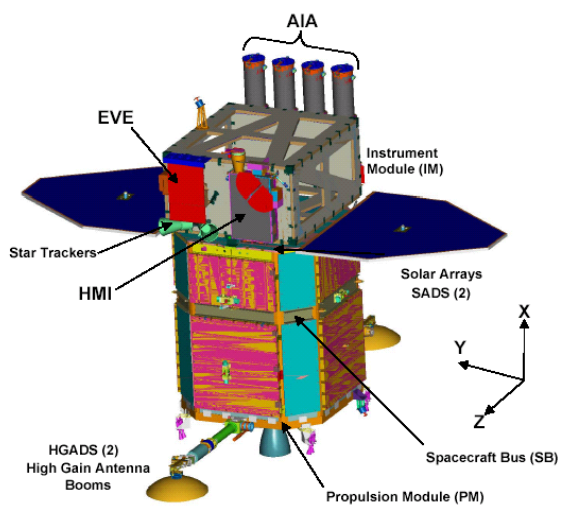

Figure 1 Solar Dynamic Observatory

The disturbance rejection capabilities of each ISS were modeled as high-pass filters. These models were verified by demonstrating that the magnitudes of the high-pass filters match the requirements on the ISS. The actual performance of each telescope's ISS was tested by engineers at Lockheed Martin. The test data were delivered to GSFC for calibrating and validating the ISS models. The left and right plots of Figure 2 illustrate the comparison between the ISS test data and the ISS model for AIA and HMI, respectively. As a note, when the test data showed

better suppression than is required, the ISS model matches the required performance in order to add some conservatism to the analysis.

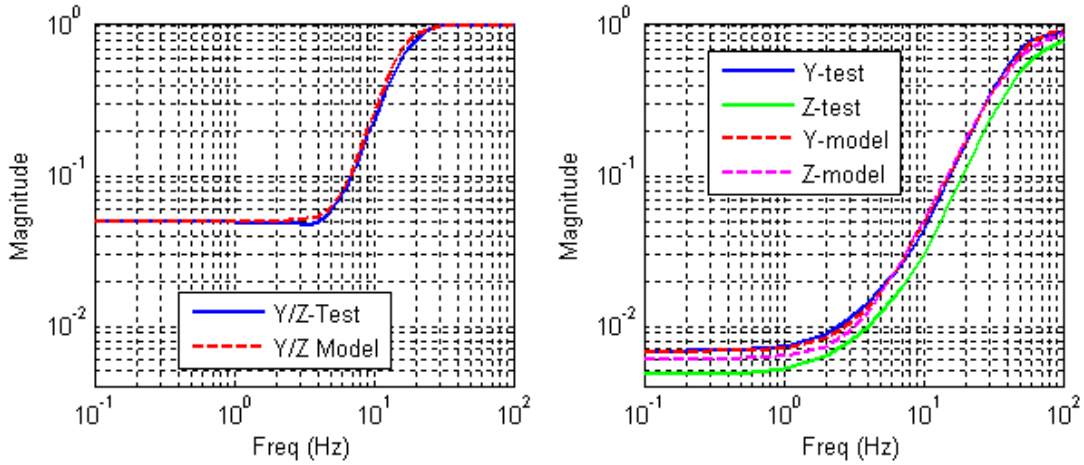

Figure 2 Attenuation transfer function: (left) AIA ISS (right) HMI ISS

C. Jitter Analysis Metrics and Margins

There are two jitter evaluation metrics used in estimating SDO jitter performance. The first metric is a frequency-domain based evaluation method defined by the SDO scientists:

$$\sigma_j = \left[\int_{-\infty}^{\infty} S_{zz}(\omega) \left| G_{\mathrm{ATF}}(\omega) \right|^2 \left(1 - \mathrm{sinc}^2(\omega\tau) \right) d\omega \right]^{1/2} \tag{1}$$

where σ_j is the root-mean-square (RMS) or 1-σ jitter, S_{zz} is the power spectral density (PSD) of the LOS motion, G_{ATF} is the attenuation transfer function (ATF) that models the ISS performance, ω is frequency in Hz, and sinc is a function defined as sinc(x) = sin(x)/x. The variable τ is the instrument exposure or integration time. The AIA telescopes have large exposure time variations that range from 0.1 sec to 3.0 sec, whereas the HMI exposure time has a smaller time range of 0.15-0.3 sec. The frequency-domain based jitter metric is appropriate for analyzing random disturbance inputs including the reaction wheel jitter analysis. However, many of the jitter sources are not random and their jitter effects can be analyzed using time-domain simulations. A second jitter performance metric used for non-random types of jitter effects is defined as follows

$$\sigma_j^2(\tau) = E\left\langle \left(\theta(t) - \bar{\theta}_\tau \right)^2 \right\rangle_\tau = \frac{1}{N-1} \sum_{n=M_1}^{M_2} \left(\theta[n] - \bar{\theta}_\tau \right)^2 \tag{2}$$

$$\bar{\theta}_\tau = \langle \theta(t) \rangle_\tau = \frac{1}{N} \sum_{n=M_1}^{M_2} \theta[n],$$

$$N = M_2 - M_1 + 1 = \frac{\tau}{\Delta t}$$

where $\theta(t)$ is the LOS motion, N is the number of sampled data points in a sliding window with width τ, M_1 is the initial index of the sliding window, M_2 is the end index of the window, and dt is the simulation sample time. The jitter prediction is calculated using either Eq. (1) for frequency-domain analysis or Eq. (2) for time-domain simulations.

There are three types of uncertainties considered in the SDO jitter analysis. The first type is the modal gain uncertainty since the magnitudes of most of the high frequency modes are not validated by test data. The second type is disturbance amplitude. Although many disturbances were measured at the component level, some

disturbance amplitudes may change after launch. To protect against the modal gain and disturbance amplitude uncertainties, the jitter analysis team aimed to achieve a 100% margin on the current best estimate (CBE) jitter when compared to the allocated requirements. The percent margin is defined as

$$\%\ \text{margin} = \left(\frac{\text{Requirement}}{\text{CBE}} - 1\right) * 100 \tag{3}$$

The third type of uncertainty is modal frequency. Typically only the frequencies of primary modes are matched to the modal survey test data, and the frequencies of other modes may easily vary 5-10% and possibly more. In order to estimate the impact of modal frequency uncertainty on the analysis results, the jitter team performed frequency sensitivity analyses by either varying the FEM modes or the input disturbance frequencies by +/- 10% . The worst-case result from the frequency sweep studies was reported as CBE to guard against frequency uncertainty. This is a source of potentially large conservatism, since the probability of perfect alignment between disturbance and modal frequency is low.

III. Reaction Wheel Jitter Tests

SDO has four Goodrich E-type reaction wheels onboard the spacecraft for attitude control. These wheels are mounted on the four upper bus panels of the spacecraft with the spin axis pointing 60 deg away from the LOS (body X) axis. The maximum torque capability of each wheel is 0.25 Nm with a momentum limit of 70 Nms. The reaction wheels are the source of high amplitude jitter disturbance, due to static imbalance, dynamic imbalance, and bearing imperfections that introduce tonal disturbances occurring at known ratios of the wheel speed. In addition, the noise signature includes a low level broadband noise characteristic that is visible at low wheel speeds. Since the net solar and gravitational torques acting on SDO are low, the wheel speed change is very slow. As a result, the wheel tonal disturbances dwells on jitter-critical observatory modes long enough to excite them to steady state.

Based on pre-launch jitter analysis estimates, the wheel speeds were limited to ±412 revolution/min (RPM) to meet AIA and HMI jitter requirements. This constraint forces the wheels to reverse direction about once every four weeks and uses only a small portion of the available wheel speed range of ±6000 RPM. As the wheel reverses direction, a small increase in LOS motion occurs and was considered an acceptable error to the science team. However, the team preferred to reduce the frequency of wheel reversals and the number of thruster maneuvers required to unload wheel momentum. The objective of the wheel jitter tests was to measure the actual wheel-induced jitter on orbit, which was expected to be smaller than the analytical prediction. If our expectation was correct, the SDO flight operations team (FOT) would be able to extend the wheel speed operational range.

A. Pre-launch Analysis

In this paper, a brief summary of the pre-test wheel jitter analysis is provided. Detailed wheel disturbance modeling, jitter analysis approach, and ground validation tests are subjects of Ref. 3. The reaction wheel induced vibration (IV) disturbances were measured by the wheel vendor in order to verify the imbalance requirements. A semi-analytical wheel disturbance model was created and tuned to the IV test data for wheel jitter analysis. This model consisted of a physical model of the wheel axial and rocking modes, including gyroscopic torques on the wheel, excited by external forces. As illustrated in Figure 3, the model has empirical tonal and broadband disturbance models, generated from fits to the IV disturbance data. The disturbances are filtered by an analytical model of the reaction wheel structural modes, which accounts for the dynamic amplification of the disturbances at wheel structural frequencies. The model development proceeded by, first, identifying the harmonic disturbances, then tuning the wheel structural modes and modal damping to match the dynamic amplification observed in the harmonic data. Finally, the harmonics were removed from the disturbance data to produce a broadband noise model.

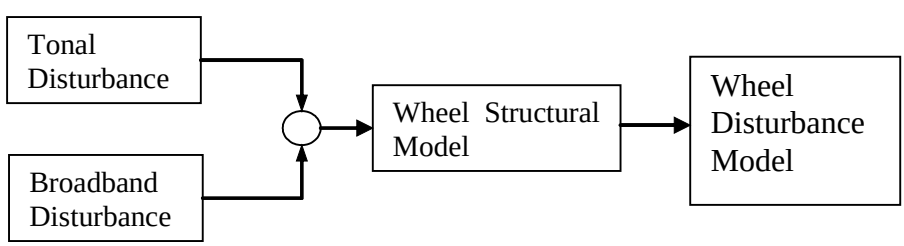

Figure 3 Semi-analytical disturbance wheel model

As an example, Figure 4 plots the torque contours about the Y axis, for one SDO wheel. The dashed lines fanning out from the lower left are the identified harmonics for the tonal disturbances. These are wheel disturbances occurring at frequencies equal to harmonics of the wheel speed. The solid black lines are the whirl modes as predicted by the physical structural model: the lower branch is the retrograde mode (precession in the opposite sense to the wheel spin), and the upper branch is posigrade. The peak disturbance occurs at several wheel speeds; at high wheel speed (above 35 rev/sec) at the fundamental, at 23 rev/sec when the second harmonic crosses the retrograde branch, and at 36 rev/sec when the 3rd harmonic crosses the posigrade branch. The wheel disturbance model predicts the whirl mode behavior well at all wheel speeds. The broadband noise from 210 to 400 Hz is particularly evident in the data set. The continuous ridge lines tracing out the whirl mode branches in the data make it clear that the wheel structural modes are constantly excited by broadband energy. Figure 5 shows an example of the radial torque power spectral density (PSD) when the wheel is running at 430 RPM. In this plot, the PSD raw data and the broadband noise PSD data are shown as a solid line and dashed-dotted line, respectively. The noise data is obtained after removing the tonal disturbances. The two dominating disturbance peaks are generated by the wheel broadband noise exciting the wheel rocking modes. A simple constant plus second-order filter model (shown as dashed line) was also developed for describing the broadband noise.

The analysis approach used for SDO was to evaluate the disturbance forces on the fixed-base wheel model, and apply these to the spacecraft structural model. This technique ignored the coupling between wheel and spacecraft structural dynamics, which could result in a shift in rocking and axial modes. The alternative of incorporating the wheel model into the FEM, and applying the gyroscopic terms to the FEM during the jitter analysis, would be more accurate but substantially more computationally intensive. To account for mode frequency uncertainty, the wheel jitter analysis allowed for a +/-10% structural mode frequency shift and reported the worst case jitter observed from the frequency sensitivity analyses. Therefore the worst-case coupling between wheel disturbances and observatory structural modes were captured. The jitter predictions and various sensitivity analyses were performed using Matlab® and Nightsky Systems Inc.'s Disturbance-Optics-Controls-Structures (DOCS) Toolbox.

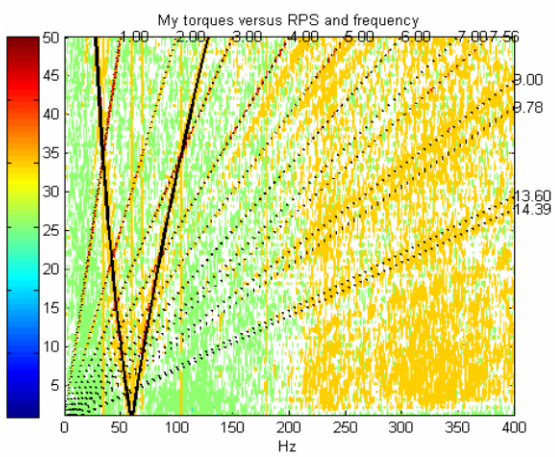

Figure 4 Contour plot of wheel torque (My)

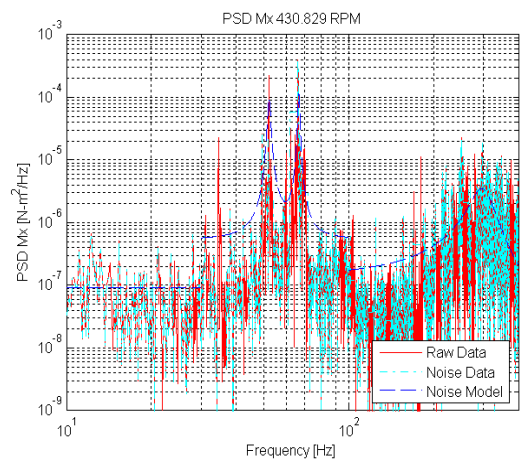

Figure 5 Broadband noise data for radial moment disturbance

After performing the wheel jitter analysis using the post-environmental wheel IV test model, the HMI LOS response exceeded the wheel 100% margin requirement at very low wheel speeds (~200 RPM). To minimize the predicted wheel jitter, a wheel location trade study was performed to place the nosiest wheel in the quietest location. In addition, the SDO team decided to conduct validation tests on the ground in order to understand the conservatism in the analysis before choosing the most appropriate wheel jitter mitigation strategy[3]. Ground wheel jitter test results showed that our analytical prediction was generally a factor of 1.5 to 2.0 larger than the measured accelerations at low wheel speeds (<700 RPM). Based on the ground validation results, the required jitter analysis margin on the wheel disturbances was reduced from 100% to 66.7% (the allowable jitter was increased by a factor of 1.33).

The latest pre-launch wheel jitter analysis predictions are shown in Figure 6 through Figure 9. There are four AIA telescopes, each with two axes of performance outputs (tip and tilt of the LOS error) which result in a total of eight jitter responses. All eight were calculated and the largest was compared against the wheel jitter allocation.

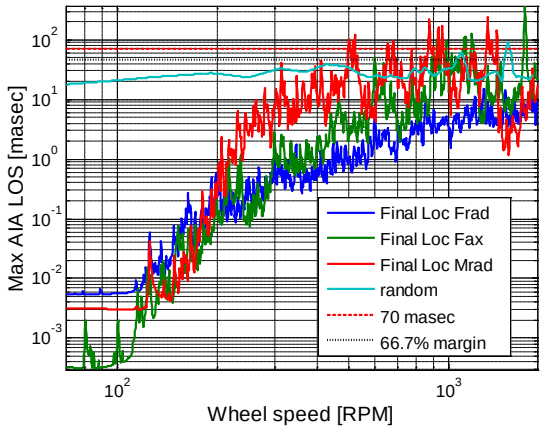

Figure 6 Maximum AIA telescope jitter due to different wheel disturbance components at final selected wheel locations

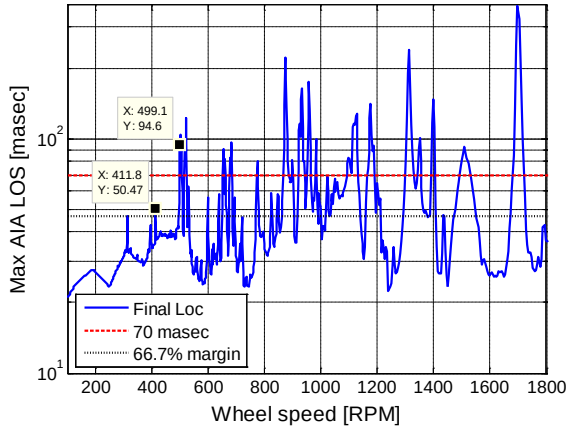

Figure 7 Maximum AIA telescope jitter due to all wheel disturbance components

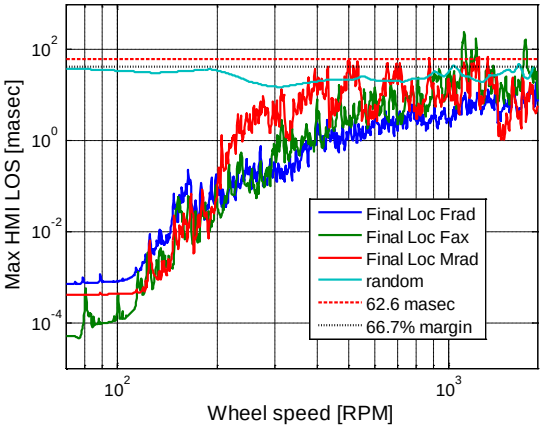

Figure 8 Maximum HMI telescope jitter due to different wheel disturbance components at final selected wheel locations

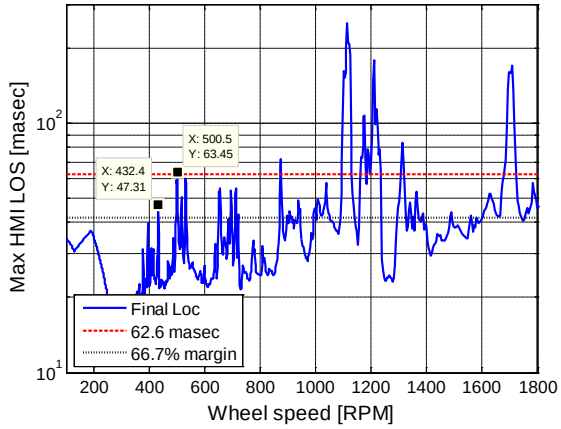

Figure 9 Maximum HMI telescope jitter due to all wheel disturbance components

Figure 6 shows the AIA jitter due to each wheel disturbance component (radial force (Frad), axial force (Fax), radial moment (Mrad), and broadband noise (random)). The 70 masec allocation and the 66.7% margin requirement (46.7 masec) are also shown as red dashed and black dotted horizontal lines in the plot, respectively. At low wheel speeds (<400 RPM), the broadband noise dominate the jitter response, whereas at high wheel speed (> 400 RPM), jitter responses due to tonal disturbances are significantly larger than those caused by the broadband noise. Since the broadband noise determines the jitter response of the telescope at low wheel speeds, it must be included in the jitter analysis. After combining all the wheel disturbance sources, the final AIA jitter response is shown in Figure 7. The wheel jitter allocation is exceeded for wheel speeds greater than ~500 RPM. The 66.7% margin allocation can be met only if the wheel speeds are limited to ~412 RPM.

For the HMI instrument, there are two performance outputs for the single telescope. The maximum jitter response over the two outputs was again computed and is reported here. Figure 8 and Figure 9 demonstrate that the HMI results follow similar trends as the AIA jitter results. The HMI wheel jitter allocation (62.6 masec) and 66.7% margin requirement (41.7 masec) is exceeded for wheel speeds greater than ~500 RPM and ~432 RPM, respectively. The pre-launch analysis results show that the 66.7% margin requirement can be met if wheel speeds are kept lower than 412 RPM for both AIA and HMI. Since SDO experiences small torques on-orbit, it is possible to run the wheels from -412 RPM to +412 RPM and still meet the four week momentum unload requirement. As a result, the

pre-launch wheel jitter mitigation plan was to limit the wheel speeds to within +/- 412 RPM during the science mode. This operating restriction obviates the need to reduce the magnitude of the wheel disturbance, for example by adding isolation systems to the wheels or the science instruments.

B. Jitter Test Descriptions

During the on-orbit wheel jitter test, all wheel speeds were driven from a slow speed (<200 RPM) to a maximum speed of about 1000 RPM. To accommodate the instrument data storage and download capabilities, the wheel speeds were accelerated during data collection periods (3 min) and held constant during data dumping periods (30 min). Furthermore, during the speed acceleration periods, the acceleration level were maintained small enough to ensure that structural modes could be fully excited (e.g. reach maximum amplitude), similar to nominal operating conditions where the wheel speeds change slowly. The acceptable acceleration level was determined to be less than 2 RPM/sec to allow sufficient time for exciting structural modes and reasonable test completion time.

The wheel speeds were varied using the reaction wheel momentum redistribution algorithm in the ACS Science Control Mode. The redistribution torque law is given by

$$\tau_{\text{red}} = -K_g \left[\frac{(h \cdot V_n)_{\max} + (h \cdot V_n)_{\min}}{2} + h_{\text{bias}} \right] V_n, \tag{4}$$

where h is the 4x1 wheel momentum vector, $V_n = [1, -1, 1, -1]$ is the 4-wheel null space vector, K_g is the momentum redistribution control gain, and h_{bias} is the parameter that can be adjusted to change the wheel momentum to the desired level. Using this control method, the wheel speed changes occur only along the null space direction and did not perturb the ACS closed-loop control torques. The parameters K_g and h_{bias} were used to achieve the desired wheel speed or momentum slew profile: K_g controlled the wheel speed acceleration level; and h_{bias} changed the wheel momentum along the null space vector. Small increments of h_{bias} were commanded to vary the wheel momentum slowly, approximating a linear momentum ramp profile (See Figure 10), until the desired momentum was reached. Figure 11 shows the desired wheel momentum slew profile during the jitter test, where the momentum was accelerated for 3 min (or 180 sec) and held constant for 30 min. The slope of the momentum change depended on the selection of K_g and the reaction wheel drag torque. Since the wheel drag torque was not well known prior to the jitter test, a separate test day was scheduled to calibrate K_g and determine the incremental size of h_{bias} to limit the speed acceleration level to 1-2 RPM/sec. The parameters chosen to achieve the desired wheel speed acceleration were: $K_g = 0.075$, and h_{bias} was divided into 10 steps between desired bias levels.

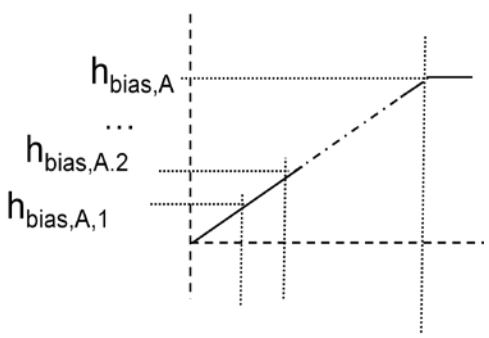

Figure 10 Momentum biases are commanded during acceleration period

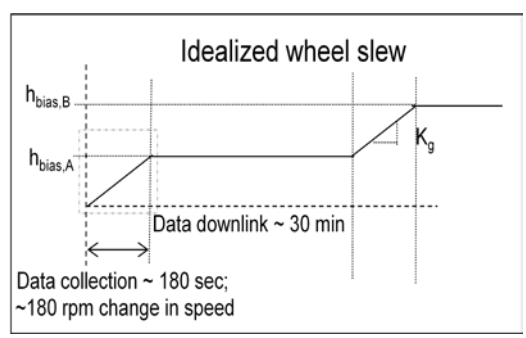

Figure 11 Wheel speed profile during wheel jitter tests

The wheel jitter test was performed in the ACS Science Mode (See Ref. 6 for more ACS control mode details). The HMI ISS control loop was opened while wheel speeds increased to ~1000 RPM and closed while wheel speeds decreased back to low levels. The open- and closed-loop test data provided the HMI team information on how well the instrument stabilization system performed. Since HMI nominally functions with a closed-loop instrument control system, jitter data collected during the speed decrement section was compared to the requirement. The AIA instrument has an open-loop instrument stabilization system as described in Section II-B. All other mechanisms, including four HGA gimbal actuators and instrument mechanisms, were held fixed during the wheel jitter test.

Part two of the wheel jitter test was planned if the analysis of the first part of the wheel jitter test showed an issue that warranted further investigation. For the wheel jitter re-test, the goal was to slew one wheel at a time in the speed range of interest while ensuring that the remaining three wheels stay inside the jitter-safe range (e.g. +/- 400 RPM). This test would identify the problematic wheel and wheel speed. The results in the following section demonstrate that a re-test was not warranted.

C. Jitter Measurements

Before examining the on-orbit wheel jitter measurements, the wheel speed and accelerations were checked to ensure the proper wheel acceleration levels were limited to less than 2 RPM/sec. The top plot in Figure 12 shows the wheel speeds of all four wheels during the test. All wheel speeds ramped up from close to 0 RPM, accelerated for ~3 minutes and held constant for ~30 minutes to download instrument data, to about 1000 RPM. The bottom plot in Figure 12 demonstrates the acceleration levels during the entire test were maintained to be below 2 RPM/sec for all four wheels.

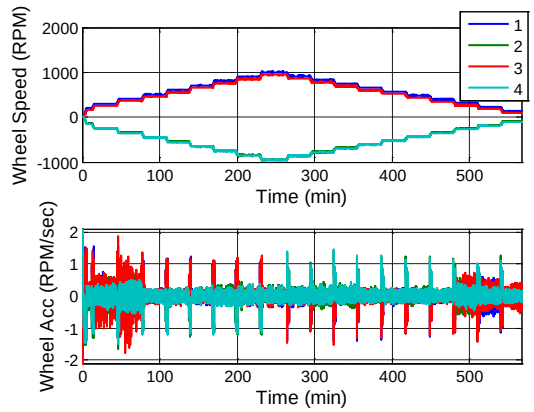

Figure 12 (top) Wheel speeds during jitter test (bottom) Estimated wheel acceleration levels

To reduce the number of data sets shown in the paper, the largest LOS measurements from all eight AIA telescope measurements (4 sensors, 2 axes per sensor) are plotted against the minimum wheel speeds (out of four wheels) in Figure 13. In this figure, the green dotted line indicates the maximum pre-launch analysis prediction for wheel speeds less than 412 RPM, and the red solid line is the wheel jitter allocation for the instrument. For the AIA telescopes, the LOS measurements were passed through an idealized filter (a factor of 20 rejection at low frequencies and a high-pass filter with a corner frequency around 4 Hz) to emulate the open-loop ISS. The results shown in Figure 13 assume the AIA ISS performed as modeled. Under this assumption, the AIA wheel-induced jitter allocation is met for wheel speeds up to at least 950 RPM. For HMI, the LOS measurements were not filtered and were collected with the ISS loop closed. The maximum HMI LOS jitter (from 2 axes) exceeds the wheel-induced allocation by less than 2.7 masec when the minimum wheel speed is between 886 and 892 RPM as illustrated in Figure 14. The on-orbit measurements show that the pre-launch maximum jitter prediction did bound the worst case AIA and HMI LOS jitter, and the wheel speed limit can be increased to 886 RPM before violating the wheel jitter allocation.

The HMI LOS measurements were further processed to compute the amplitude spectra. The entire measurement is divided into 12-sec time segments, where the amplitude spectra for four 3-sec segments were computed and averaged. During each time segment, the wheel speed was considered quasi-static with the mean wheel speed calculated. The amplitude spectra versus mean wheel speed and frequency is shown as a contour plot in Figure 15. For ease of visualization the logarithm of the amplitudes are plotted, not the actual amplitudes. The spectral analysis clearly demonstrates the wheel rocking modes effects at low wheel speeds (< 500 RPM) and tonal harmonics crossing the rocking modes at higher wheel speeds. These results emphasize the importance of including rocking mode excitations by the broadband noise in the reaction wheel disturbance model. Figure 15 also shows a notable constant disturbance at around 210 Hz which does not vary with wheel speeds. This disturbance frequency was not observed in the wheel component test data. Since all other disturbance mechanisms were turned off during the wheel jitter test, the source of the 210 Hz disturbance remains unclear.

D. Summary and Jitter Mitigation Applied

The on-orbit jitter measurements allowed the SDO team to extend the wheel speed jitter limit to +/- 850 RPM instead of +/-412 RPM. Since the wheels can accumulate more momentum with the larger speed limit range, the period between thruster momentum unloads will be greatly increased. The number of direction reversals each wheel will experience over its lifetime will be reduced, minimizing mechanical wear of the wheels at low speeds.

For all other jitter tests, the wheel speeds were maintained below 300 RPM to keep wheel-induced jitter low. Table 1 provides a summary of the largest LOS measurements under 300 RPM. These values are combined with predictions and allocations when compared with on-orbit jitter measurements for other jitter tests.

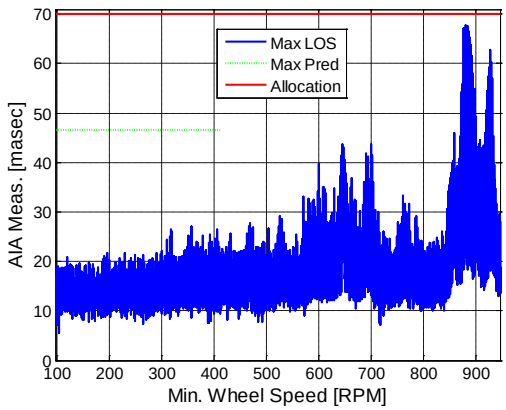

Figure 13 Max. AIA LOS jitter measurments

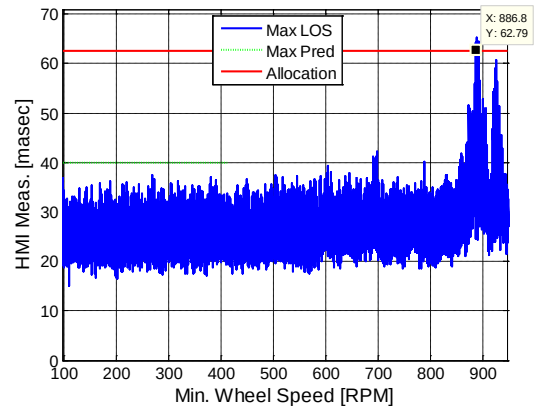

Figure 14 Max. HMI LOS jitter measurements

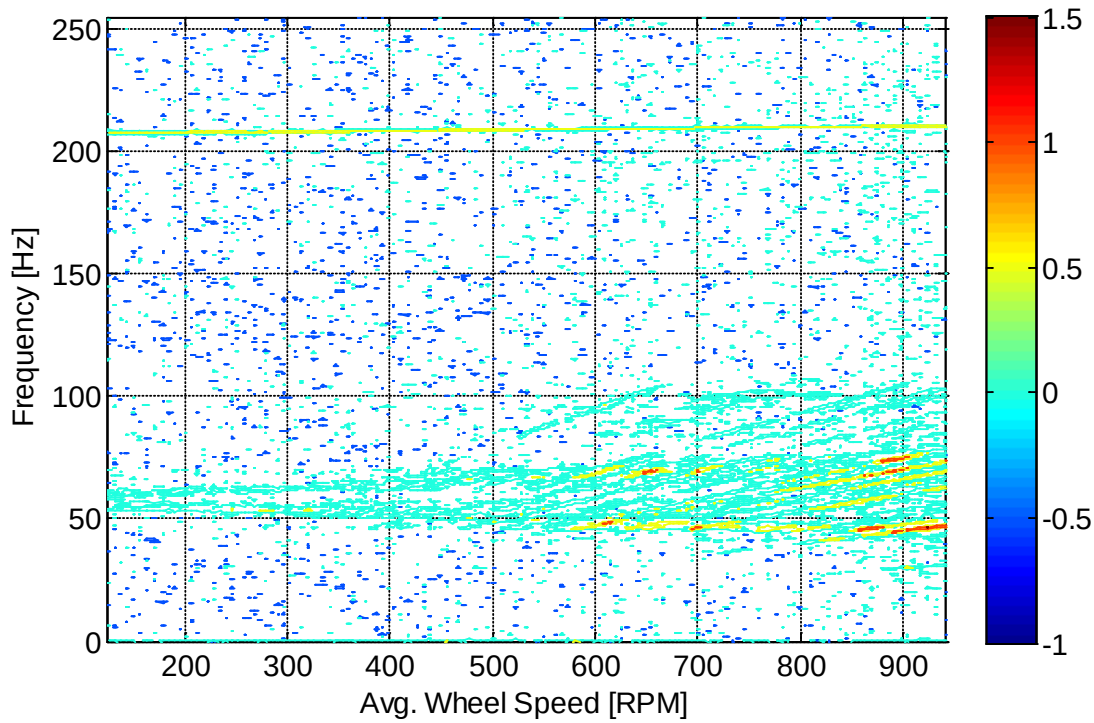

Figure 15 Contour plot of HMI measured jitter vs. frequency and wheel speeds

Table 1 Wheel jitter bound under 300 RPM

Instrument/Axis	Jitter Bound [masec]
HMI LOS Y	35
HMI LOS Z	25
AIA1 LOS Y / Z	10
AIA2 LOS Y / Z	20
AIA3 LOS Y / Z	20
AIA4 LOS Y / Z	10

IV. High Gain Antenna (HGA) Jitter Tests

Preflight analysis indicated that the HGAs would be one of the largest disturbance sources on-board the spacecraft. The disturbance arises from the near-impulsive torque imparted as the HGA actuators step, producing torques at the step rate and at integer harmonics with gradually decreasing magnitude, up to the armature natural frequency. The HGA actuators are stepper motors integrated with a 200:1 harmonic drive gearbox, with a step size of 0.0075 degrees. There are four actuators, comprising azimuth and elevation axes for the two (+Z and –Z) HGA antennas. They track, where the dish is pointed at the White Sands ground station target, and slew, where the dish is moved from one target to another during the handover season[4]. The actuators move at a relatively slow rate during tracking (up to 3 steps per second) and slewing (5.2 steps per second), which allows the jitter response from one step to decay somewhat before the next step is taken. Therefore the jitter response is largely determined by the response to a single step. Since the response does not decay to zero over that time, there is the possibility of interaction between steps, which can add the responses from successive steps.

As a result of the potential for problematic HGA induced jitter that was identified during pre-launch analysis, several jitter mitigation algorithms were implemented to reduce the jitter response due to step interaction: random step delay, stagger stepping, and the HMI No-Step Request (NSR) flag. Random step delay causes each commanded step of each of the 4 actuators to be delayed for a certain pseudo-random number of counts, so that actuator pulses at a constant rate do not "ring up" critical modes. Stagger stepping forces the +Z and –Z actuators to operate in staggered ACS cycles, so that simultaneous +Z and –Z actuator commands do not interact to produce increased jitter. The NSR flag, when issued by the HMI just prior to acquiring an image, requests a one-exposure-long delay before any of the actuators are commanded to step. The goal of the HGA flight jitter measurement was to see if the actual jitter was low enough to allow one or more of the mitigation algorithms to be switched off. Note that all of the mitigation strategies delay the motion of one or more gimbals. The peak rate required to follow the nominal antenna pointing profile is 43 degrees per hour. However, since the mitigation algorithms cause the gimbals to lag the desired profile, the actuators must be allowed to move at a higher than nominal rate (as much as 140 degrees per hour) in order to catch up to the desired profile after a delay.

The largest jitter response seen in pre-flight analysis was two times the single-step response, depending on the precise timing between sequential steps. A jitter dependence on HGA angle was also found as the coupling to various jitter-sensitive modes changed. Therefore, the test strategy employed to assess the jitter level on-orbit was to measure the single-step response to moves of each of the four actuators, at a range of joint configurations.

The allocations to HGA induced jitter are 106 masec of the AIA's overall pointing budget, and 94 masec of the HMI's. The AIA has a 95% data continuity budget (5% of the images can be degraded, and the science requirements will still be met). This budget was all allocated to HGA induced jitter, so the HGA requirement is that the AIAs meet the 106 masec allocation for at least 95% of the time. The HMI has an image registration requirement (sequential images are batch processed), so that no image can exceed the jitter requirement without causing the entire sequence to be lost. Therefore the HMI requirement must be met for every image.

A. Pre-launch Analysis

The pre-launch jitter predictions were created using a time-domain simulation of the SDO structural dynamics model, running inside a MATLAB® Simulink® nonlinear model of the stepper motor actuators. The actuator simulation was based on a Simulink model developed by the motor manufacturer, SpaceDev of Durham, NC, for loads analysis. The model includes the nonlinear unpowered holding (detent) torque, the powered holding torque, and friction acting on the rotor and output shaft[2]. The SDO structural dynamics model was used for the HGA jitter analysis. The unpowered armature has a natural frequency of 66 Hz, which increases to 72 Hz when the windings are powered.

The structural dynamics model was verified using a number of component and integrated tests, including modal testing and tap testing of the system at various levels of integration. The HGA model was calibrated and verified using a number of tests. The actuator model was verified using measurements of the winding voltage and current during operation, which provided data about the electrical and mechanical response of the system on the drive side of the gearbox (the winding electrical dynamics and the rotor ringing). The actuator was operated on a dynamometer (a Kistler 6DOF force measurement table) to verify the behavior outside the gearbox (the effective gearbox stiffness). A tap test was also performed on the HGAS antenna, to verify the HGAS Finite Element model natural frequencies. Finally, the entire HGA subsystem (boom, actuator, flight dish) was mounted to the Kistler table and driven through representative profiles to verify the Simulink jitter analysis[2].

The AIA and HMI instruments incorporate active steering mirrors that partially compensate for LOS error, up to about 20 Hz. The ISS reduces low-frequency error, so that the jitter is dominated by the response in the 40-60 Hz

frequency range. This response is exacerbated by the fact that the telescope was designed to be as stiff as possible, with the result that all of the modes of the bus and the instruments start around 30 Hz, leading to multiple closely spaced modes in the 50 to 70 Hz range, which reinforce each other and lead to dynamic response that is 4-5 orders of magnitude larger than an equivalent inertia rigid body. Note that this is also where armature dynamics come into play.

Since the finite imaging time acts to filter out jitter response below a certain frequency, a moving average jitter computation is performed to account for the effect of the imaging processing (see Eqn 2). Representative exposure times are assumed; 0.1, 0.3, and 0.5 seconds for the AIA, 0.15 seconds for HMI. For each exposure time, a section of time response data equal to the exposure time is taken, the mean is removed, and RMS response is computed. The time window is then advanced one sample time, and the computation repeated. The result is a time history of the moving average RMS over the specified exposure time. The peak jitter over the entire profile is extracted, corresponding to a worst-case alignment of an exposure with the HGA induced jitter.

Figure 16 plots the AIA peak single-step predicted response from the post-CDR model generation as a bar chart. Each of the four groups corresponds to one of the actuators. Each of the bars in the group associates to one of six model configurations, with a corresponding set of four actuator angles listed as +Z azimuth, +Z elevation, -Z azimuth, and -Z elevation. For all but one of the models, the nominal fuel level is assumed in the model, with one model assuming a 5% full fuel level. Note that there is a significant variation in the jitter level imparted by each of the actuators, from 20 to 103 masec. The +Z elevation actuator generally produces the highest jitter over all configurations. That actuator also has significant variation with configuration, from 80 to 103 masec. Other actuators, while having a lower peak jitter, have a proportionally greater change in jitter with configuration. The range is not due to the variation of static inertia of the antenna, but to the way that the actuator couples into observatory modes in the 50-70 Hz range. Therefore the peak jitter is not a smooth function of joint angle.

The predicted HMI jitter is shown in Figure 17. The jitter is presented for the shortest (worst case) exposure time, for single step responses from each of the 4 actuators, for the same six configurations as previous. It varies from less than 20 masec for the azimuth actuators, to 69 masec for the +Z elevation actuator, quite a bit lower than the AIA peak jitter. The variation with actuator configuration is generally lower than for the AIAs as well. As will be shown, the actual HMI jitter has significant variability with configuration. The AIA model is quite detailed, but the HMI model is less so, and this is likely leading to incorrectly modally sparse behavior in the critical frequency range for the latter instrument.

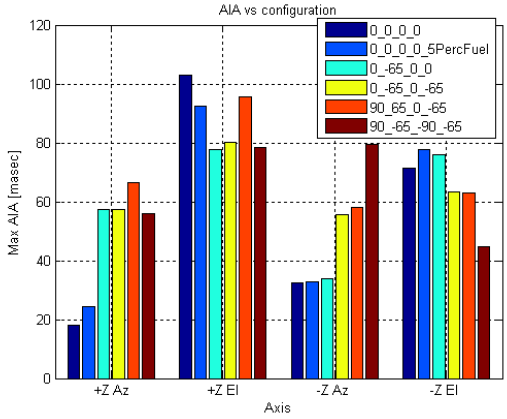

Figure 16 Pre-launch prediction of HGA-induced AIA jitter for a single step (maximum over telescope and axis).

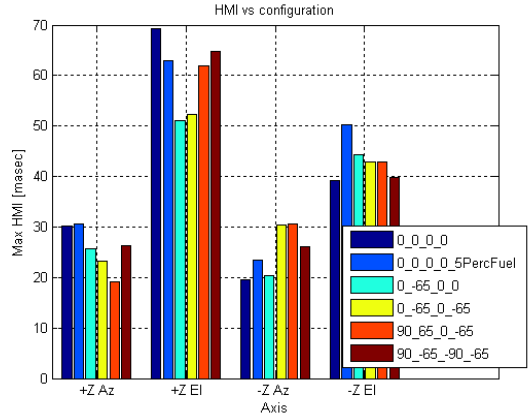

Figure 17 Pre-launch prediction of HGA-induced HMI jitter for a single step (maximum over axis).

B. Jitter Test Descriptions

The HGA on-orbit jitter test consisted of a sequence of moves of each antenna independently. Two stepping profiles were tested: single steps of each of the four actuators, and a sweep through the actuator rates from zero to the maximum tracking rate of 140 degrees per hour. The inactive antenna was put in the home position (azimuth and elevation gimbals are at 0 deg). The other was slewed to a defined starting angle. At each angle, the actuator was commanded to take two steps in azimuth and two in elevation, with a 10 second dwell between steps to ensure that the response has decayed before the next step is taken. Then the swept rate test was performed. The swept rate test

was intended to find the peak jitter as a function of step rate. The actuators could not be stepped at a continuously varying rate, so a set of constant rate segments was used. Eleven rates between 13.5 and 140 degrees per hour (0.5 to 5.2 steps per second) were commanded. Each step rate was held for 10 seconds. The total distance moved during the test was 1.7 degrees. The antenna then moved at maximum slew rate to the next test configuration, then dwelled to allow the observatory to quiet. The starting configurations were taken from the azimuth at 90 degree intervals, and the elevation actuator at (-45, 0, 45) degree configurations. A total of 23 configurations (encompassing +Z and -Z moves) were tested.

The jitter was measured using the same instruments as for the reaction wheel tests. The wheels were operating at low speed during the HGA test, with a small but non-negligible contribution. The maximum jitter introduced by the wheels, as determined by post-launch data processing, is given in Table 1. The tests were run with the No-Step Request flag, the stagger step flag, and the step delay flags off (algorithms not operating), in order to ensure that the gimbals achieved the desired step rates.

C. Jitter Measurements

The measured single-step AIA jitter is plotted in Figure 18. Two aspects are immediately apparent. First, the peak jitter is significantly higher than the pre-launch prediction shown in Figure 16, 140 masec versus 103 masec. The ratio, indicating the magnitude of the prediction error, is 1.35. Second, there is more variability in the elevation actuator induced jitter than indicated by the pre-flight model, from a minimum of 45 to a maximum of 140 masec, compared to the prediction of about 80 to 103 masec. The azimuth induced jitter, by contrast, shows less variation with configuration than the prediction. The measurements also indicate that a 180 degree flip of the gimbal has a significant effect on the induced jitter magnitude.

The Power Spectral Density (PSD) of the AIA response for the (0,0,0,0) configuration is plotted in Figure 19. The blue curve is the predicted PSD, and the green curve is the measured PSD. The top plot shows the running integral of the PSD, thus indicating the frequency ranges which contribute most of the energy to the response. The plots show that the dominant source of energy is in the 50-60 Hz range. The pre-launch prediction captures the frequency range that dominates jitter, but under-estimates the magnitude.

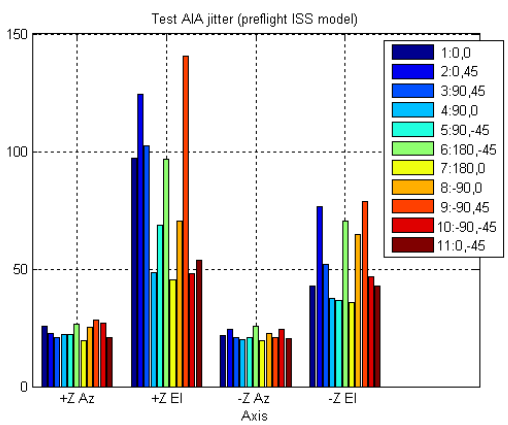

Figure 18 Measured HGA-induced AIA jitter for a single step (maximum over telescope and axis).

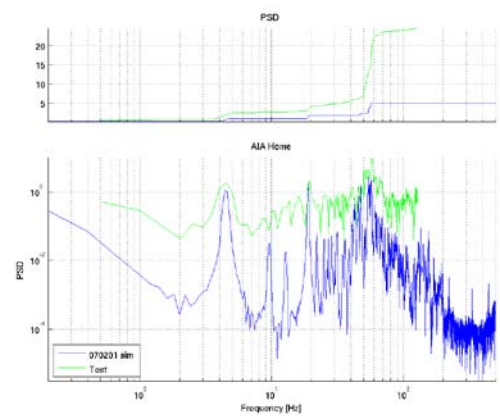

Figure 19 PSD of peak AIA response for the home configuration, simulation (blue) and measurement (green).

The measured single-step HMI jitter is plotted in Figure 20. The maximum single-step jitter is 165 masec, induced by the -Z elevation actuator at the (180, -45) configuration. The peak predicted jitter is 69 masec, implying a prediction magnitude error of 2.4. As mentioned previously, this error is due to the use of an insufficiently detailed model of the HMI in the observatory FEM. Figure 21 shows the PSD for the HMI jitter at the (0,0,0,0) configuration. Blue is the prediction, green is the measurement. Once again, the prediction captures the frequency range dominating the response, but significantly under-predicts the magnitude.

The pre-launch prediction was that the peak jitter during constant rate operation was approximately 2 times the single-step jitter. The maximum of the AIA moving average responses during the acceleration slew was 2.6 times higher than the peak single-step response. The peak HMI slew response was 1.9 times the peak single step response. The higher measured ratio is due to the fact that the tests were conducted with all the mitigation algorithms disabled.

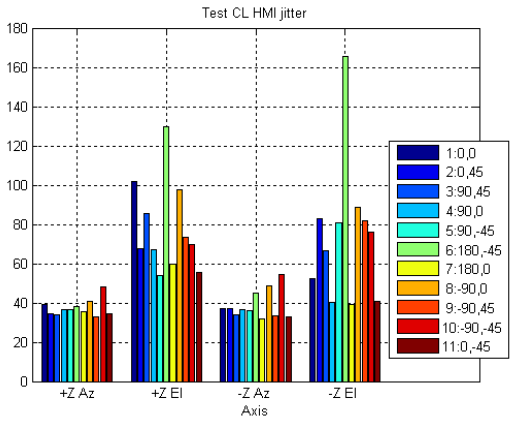

Figure 20 Measured HGA-induced HMI jitter for a single step (maximum over telescope and axis).

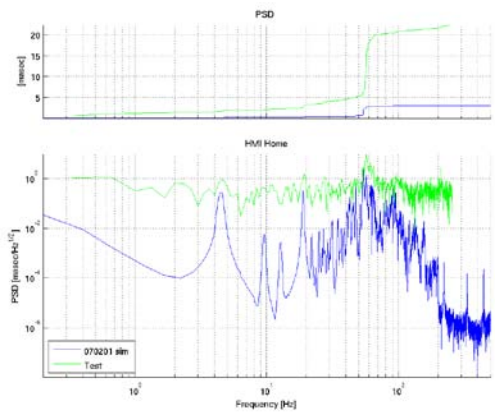

Figure 21 PSD of peak HMI response for the home configuration, simulation (blue) and measurement (green).

D. Post-test Analysis

The flight measurements show significant variation in jitter with respect to configuration. Pre-launch analysis evaluated different configurations than were run during the flight measurements. It is therefore impossible to separate prediction differences due to model error from differences due to configuration. In order to isolate the effects of model error, the jitter analysis was repeated, post-test, for the angles that were tested in flight. The finite element model was used to create a Normal Modes representation for each of the 22 configurations tested. The model was identical to that used for the pre-launch analysis, with the exception of the joint angles. The single-step jitter analysis was repeated for each configuration.

The simulated and measured single step jitter for the 22 flight configurations are plotted in Figure 22 (AIA) and Figure 23 (HMI). For each plot, the vertical axis shows the joint configuration, the green and blue bars are the measured response to elevation and azimuth steps, respectively, and the magenta and red bars are the simulated response to elevation and azimuth steps, respectively. Note that only one of the HGAs (+Z or –Z) was tested at one time, corresponding to the boom with non-zero joint angles. So, for the first 10 configurations, with the +Z antenna at home and the –Z antenna slewed to the starting angles indicated, the two actuators on the –Z boom were stepped. Examining the AIA results, the simulation generally produces acceptable predictions. The largest responses come from the elevation actuator, and the simulation response is almost always larger than the measured response, as desired. The largest simulated response exceeds the largest measured response, although they occur at different configurations.

The result is different for the HMI (Figure 23). Here, the elevation actuator produces the largest response, as before, but the measured response exceeds the simulation response for most cases. Additionally, the simulation predicts that the largest responses, on average, come from the +Z boom. However, the measurements show that the –Z boom produce the larger HMI response. As mentioned previously, the HMI response was less detailed than the AIA response. It is likely that the coarse HMI model did not have the fidelity needed to capture the modal structure within the instrument that is excited by the 50-70 Hz actuator disturbances.

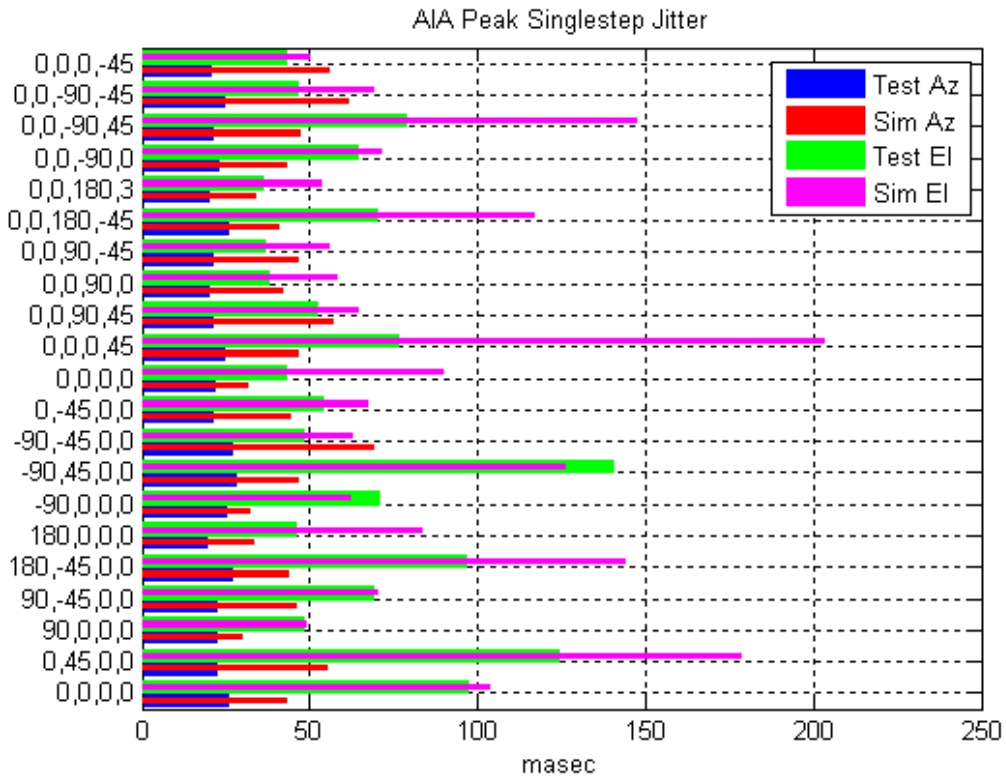

Figure 22 Measured versus post-launch simulation of single-step HGA-induced AIA jitter.

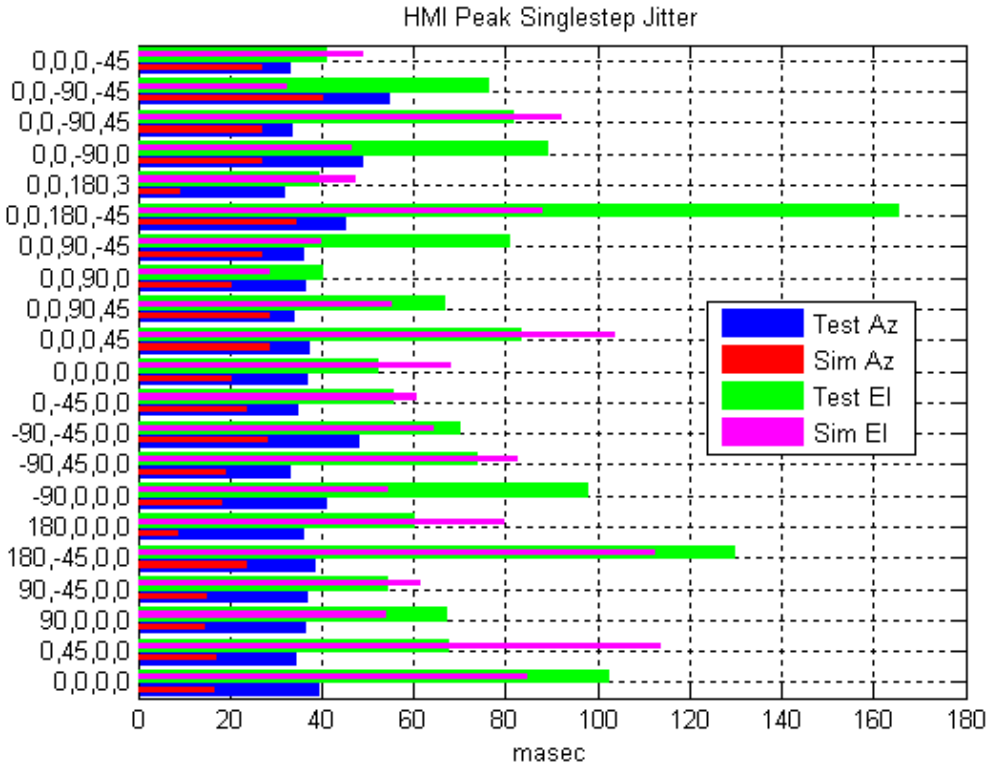

Figure 23 Measured versus post-launch simulation of single-step HGA-induced HMI jitter.

E. Summary and Jitter Mitigation Applied

The summary of the measured HGA induced jitter is shown in Table 2. The table shows the moving average responses of the four AIA telescopes, and the HMI telescope, in both Y and Z axes, in units of masec. The shortest (worst-case) exposure times are used, 0.1 second for AIA and 0.15 seconds for HMI. The cases presented for the test results include the peak jitter over configuration for azimuth and elevation single-step, and the rate slew test. For AIA, the numbers represent the 95% LOS jitter, that is, a value for which the LOS is lower 95% of the time. For HMI, the response given is the peak response. For all test cases, the reaction wheel disturbances given in Table 1 are assumed to be present, at their bounding values, and are subtracted out in quadrature. The cases presented from the simulation are the maximum single-step jitter from azimuth and elevation actuator steps. The table also shows the allocation, and the margin computed from the test 95% (for AIA) and peak (for HMI). When the test value is lower than the allocation, the margin is the requirement divided by the test minus 1. When the test value is above the allocation, the margin is the test divided by the requirement minus 1.

The AIA results show better margins than the HMI, as was suggested by the single-step jitter results comparison. The worst jitter response occurs for the ATA 3 telescope in the Z axis, which at 130.7 masec is 23.3% over the 106 masec allocation. There is only one other negative margin, for the ATA2 telescope in the Z axis. These axes of these two telescopes were found in the pre-launch analysis to be the most sensitive to HGA jitter. The HMI jitter is substantially higher. Both axes have negative margin, with the Y axis 20.3% above the requirement and the Z axis high by 120.4%. This is partially due to the use of the peak jitter rather than the 95% jitter level, and partially due to higher HMI jitter for the same actuator disturbance.

Table 2 HGA induced jitter summary [masec]

Case		ATA1		ATA2		ATA3		ATA4		HMI	
		Y	Z	Y	Z	Y	Z	Y	Z	Y	Z
Test	Az	15.9	13.0	9.9	19.8	14.2	15.8	13.1	13.5	41.9	26.6
	El	36.7	71.7	37.4	139.1	38.0	136.9	44.5	77.0	88.3	163.4
	95%/Peak	41.3	71.1	39.1	122.4	44.1	130.7	45.6	75.5	113.1	207.2
Sim	Az	68.7	61.5	45.0	32.4	43.3	33.5	45.3	38.5	20.9	40.1
	El	91.5	76.5	203.0	72.1	197.5	75.0	101.8	42.6	113.4	36.4
Alloc		106.0	106.0	106.0	106.0	106.0	106.0	106.0	106.0	94.0	94.0
Margin		156.8	49.0	170.8	-15.5	140.2	-23.3	132.7	40.4	-20.3	-120.4

The comparison of single-step prediction to measurement shows that there is some model error. The peak measured AIA response is as much as 1.8 times higher than the prediction, while the peak HMI response is as much as 4.5 times higher. The error in both instruments arises because the model does not correctly capture the interaction of the observatory modes and the actuator disturbance harmonics (due to errors in modal spacing and/or modal gain). The HMI error is larger because the coarse finite element model exacerbates these characteristics.

The HGA jitter tests show that flight measurements are higher than pre-flight predictions at various HGA joint configurations, despite several levels of analysis conservatism, on assumed damping and reserved margin. As a result, HGA jitter mitigation options (stagger-stepping and NSR flags) were enabled to meet instrument LOS jitter requirements. As discussed extensively in Ref. 4, the mitigation algorithms work as expected and greatly reduce HGA-induced jitter in science images.

V. EVE Instrument Filter Wheel Jitter Test

The EVE instrument contains four filter wheel (FW) mechanisms that weigh less than two lbs each. Each FW rotates to one of five positions right before science imaging time. Its rotation usually takes two seconds to traverse from one filter position to the next, subtending an angle of 72 deg, and to rewind from the final filter to the first requires ten seconds to complete. This is accomplished by a stepper mechanism that operates at a nominal rate of 125 pulses/sec (PPS), but the step rate can be varied on orbit. Its spin axis is parallel to the SDO LOS (X-axis) that points toward the sun. The EVE FW is the third largest disturbance contributor after the HGAs and the reaction wheels. Since EVE does not have tight jitter requirements, the jitter team was not concerned by the EVE self-induced jitter, but the FWs can induce large mechanical vibrations in the AIA and HMI science instruments.

The EVE FW operates much less frequently than wheels and HGA gimbals. Each FW is expected to move only 10 seconds per day in a 40-min window. Although the FWs move infrequently, the HMI science data can still be significantly impacted by the FW-induced disturbances. For example, a short period (e.g. seconds) of large jitter can cause HMI to lose an entire 4-minute data record. If HMI loses one or two 4-minute data records every day due to EVE FW movements, it cannot meet its data continuity requirement. Based on pre-flight jitter analysis, large jitter disturbances are expected to occur only if the EVE FW step rate coincides with one of the observatory structural modes. During the on-orbit jitter test, the SDO jitter team varied the EVE FW step rate to investigate if the nominal rate (125 PPS) caused larger LOS errors than other available step rates.

A. Pre-launch Analysis

The pre-launch EVE FW analysis was first performed using a simple, physical-based stepper motor model, applying torque only around the spin axis. However, the EVE stepper mechanism contained internal dynamics that can only be revealed by test data. To more accurately characterize the disturbance forces and moments, a test of the mechanism was conducted at GSFC where the FW induced-forces and moment were measured at various spin rates. Figure 24 shows the FW mechanism mounted on a Kistler dynamometer table. A representative set of test data collected at 125 PPS is shown in Figure 25 for the spin axis torque. This figure also illustrates the amplitude spectrum of the spin-torque data, where the peak disturbance occurs at the spin rate frequency. The actual disturbance data contains three-axis force and moment disturbance with a wide range of harmonics. Some may be due to anti-backlash gears operating at high frequency. The jitter team decided that the mathematical model developed was unable to accurately duplicate the test[5]. Thus, the test data was used directly in the spacecraft jitter analysis, ignoring the simple model of the stepper mechanism.

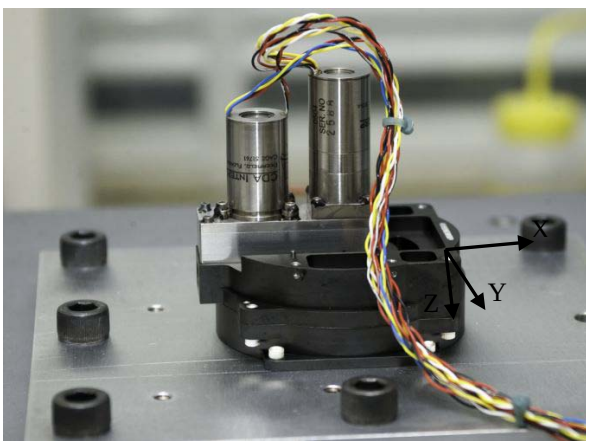

Figure 24 EVE Filter Wheel Test Set-up

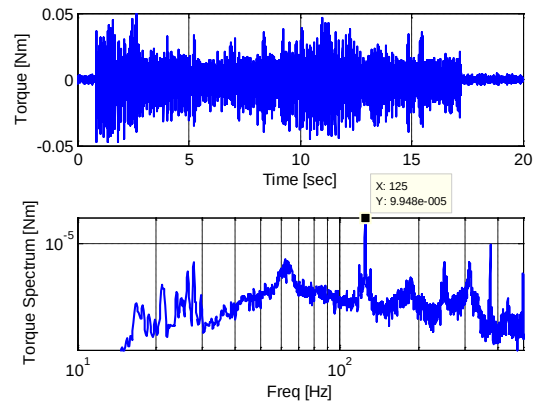

Figure 25 (top) Spin-axis torque data (bottom) Amplitude spectrum of torque data

The EVE FW pre-launch jitter analysis was a straight forward transient response analysis where forcing functions were applied directly to the observatory dynamic model and displacement responses were computed. The disturbance test data were used directly as forcing functions. It should be noted that only one of the four FWs was tested to provide disturbance measurements. In addition, the EVE dynamic model is a simple lumped mass on the spacecraft with no detailed mechanism and instrument modeling. The pre-launch analysis was performed by applying the measured disturbances for one FW at the EVE lump mass node. This analysis did not include a model uncertainty factor but is required to meet the allocation with 100% margin as presented in Section II-C. In order to account for frequency uncertainty in the FEM, a +/-10% of model frequency smearing was performed by a simple scaling of the mode frequency in 1% increments (e.g. 0.90, 0.91, … 1.01, 1.02) and repeating the time-domain transient analysis for all cases. There is no guarantee that the maximum or minimum point is located by the chosen frequency scaling, but the combination of the worst-case frequency sensitivity result with the required analysis margin was expected to bound the actual maximum LOS jitter induced by EVE FWs.

The effect of how FW step rates impact performance was studied using four rates that would be tested on-orbit: 125 (baseline), 111, 100, and 91 PPS. For each rate, the entire analysis was repeated, including all frequency sweeping/scaling. From the frequency sweeping results, the largest values were chosen as pre-launch predictions.

Table 3 shows the range of these predictions over the four stepper rates which can vary by a factor of two depending on step rate. The largest HMI LOS jitter prediction is slightly higher than the self-imposed 100% margin against EVE-induced jitter allocation. This exceedance provided another motivation for testing the EVE FW at different rates on orbit to ensure that the nominally chosen rate does not exceed the jitter allocation.

Table 3 Range of pre-launch EVE FW induced jitter from all step rates

	LOS Jitter (masec, RMS)		
	Prediction	Allocation with 100% margin	Allocation
AIA LOS (masec)	12.0 – 31.8	32	64
HMI LOS (masec)	15.5 – 29.8	24.7	49.4

B. Jitter Test Descriptions

Each of the four EVE FW was commanded to spin at a pre-specified rate for a full revolution while the AIA and HMI sensors recorded jitter data. The four specified test step periods were 8, 9, 10, and 11 milli-seconds which corresponded to test rates of 125 (nominal), 111.1, 100, and 90.9 PPS.

At each step rate, the four filter wheels were commanded to rotate a full revolution (~10 seconds), one at a time. There was about a five second rest time injected between each wheel rotation. The following table details the test sequence:

Table 4 EVE filter wheel jitter test sequence

Start	*time required*	*Stop*	
00:00.0	00:30.0	00:30.0	Start AIA/HMI Diagnostic Mode
00:30.0	00:01.0	00:31.0	Start EVE RTS command
00:31.0	00:09.6	00:40.6	Rate 1/EVE FW 1
00:40.6	00:05.0	00:45.6	Dwell time
00:45.6	00:09.6	00:55.2	Rate 1/EVE FW 2
00:55.2	00:05.0	01:00.2	Dwell time
01:00.2	00:09.6	01:09.8	Rate 1/EVE FW 3
01:09.8	00:05.0	01:14.8	Dwell time
01:14.8	00:09.6	01:24.4	Rate 1/EVE FW 4
01:24.4	00:05.0	01:29.4	Dwell time
01:29.4	14:54.0	16:23.4	Stop data collection and download data
16:23.4	10:00.0	26:23.4	Down time between tests

To provide multiple data samples for analysis, each step rate was tested three times, so the above sequence was repeated three times.

The EVE FW jitter test was performed in the ACS Science Mode. During this test, the reaction wheel speeds were kept low (<~300 RPM), and other disturbance sources (HGA, AIA mechanisms, and HMI mechanisms) were stopped in order to isolate the FW disturbance signatures. The HMI instrument ISS loop was closed to emulate nominal operating condition.

C. Jitter Measurements

The EVE jitter test LOS errors for AIA and HMI are shown in Figure 26 and Figure 27, respectively. In both figures, the blue solid line is the LOS error measurement which includes both wheel and EVE FW disturbances. During this test, the wheels were operating at low speeds (<300 RPM) to minimize wheel-induced jitter while varying the chosen EVE FW step rates. The black vertical lines separate the test periods for the four different FW step rates. Within each test period (or two vertical lines), the start time of each FW's rotation is marked by a star symbol. Groups of four stars appear in the figures demonstrating four FWs rotating sequentially. Since each rate test was repeated three times, three groups of four stars appear between black vertical lines.

For comparison to analysis prediction, the largest wheel-induced jitter measurement, less than 300 RPM in Table 1, was added to the pre-launch, worst-case EVE FW jitter prediction as shown by the green dotted line. The same largest wheel measurements were also combined with the instrument jitter allocations, plotted as the red solid line in Figure 26 and Figure 27. The AIA measurements in Figure 26 show the pre-launch prediction does bound the largest LOS error for all four FW step rates, and the EVE mechanism jitter allocation is met. The jitter level sensed by HMI is much higher than AIA during the EVE FW jitter test as shown in Figure 27, since HMI and EVE are mounted on the same +Z face of the SDO instrument deck, where as AIA is mounted on the opposite side (-Z face) of the deck. The HMI LOS errors are above the pre-launch worst-case prediction but below the jitter allocation for three tested rates (125, 111, and 91 PPS). The jitter allocation is only slightly exceeded for the 100 PPS rate.

By comparing the star markers that denote the mechanism start times to the LOS measurements, it is clear that the four FWs do not generate equal amount of disturbances. For HMI LOS and a EVE FW rate of 125 PPS, FW #4 appears to generate more jitter than the first three wheels. This behavior could partly due to the fact that the jitter generated by the first three FWs had not completely subsided and interacted constructively with the fourth FW disturbances to create more jitter. However, given all three FW #4 movements showed an increased jitter level, it is very likely that the FW #4 does generate a higher disturbance level at 125 PPS by exciting an observatory mode that negatively impacts the HMI LOS. Similarly for a step rate of 111 PPS, FW #1 and #4 create larger HMI jitter than FW #2 and #3. Since the EVE dynamic model did not model the four FW mechanisms separately, the pre-launch analysis could not have predicted the LOS jitter variations generated by the different FWs. In addition, the HMI model has less model fidelity (as discussed in Section IV) than AIA, so the HMI dynamic behavior around the EVE step rate frequencies (91-125 Hz) was probably not characterized accurately enough to capture the high frequency dynamic interactions with the EVE FWs. With that said, if the team uses a step rate of 91 PPS to operate the EVE FWs, the HMI measured response would be significantly lower than using other step rates.

The amplitude spectra of the HMI LOS measurements were computed to understand the frequency content of the jitter response. As illustrated by Figure 28, the primary disturbance response occurred at the FW step rate frequency as predicted in the pre-launch analysis. Harmonic disturbances with frequencies higher than the HMI sensor Nyquist frequency (256 Hz) are aliased, but their amplitudes are much smaller than the amplitude at the selected step rate. The unknown persistent LOS error around 210 Hz, seen previously in the RWA jitter response, is again present in the amplitude spectrum plot.

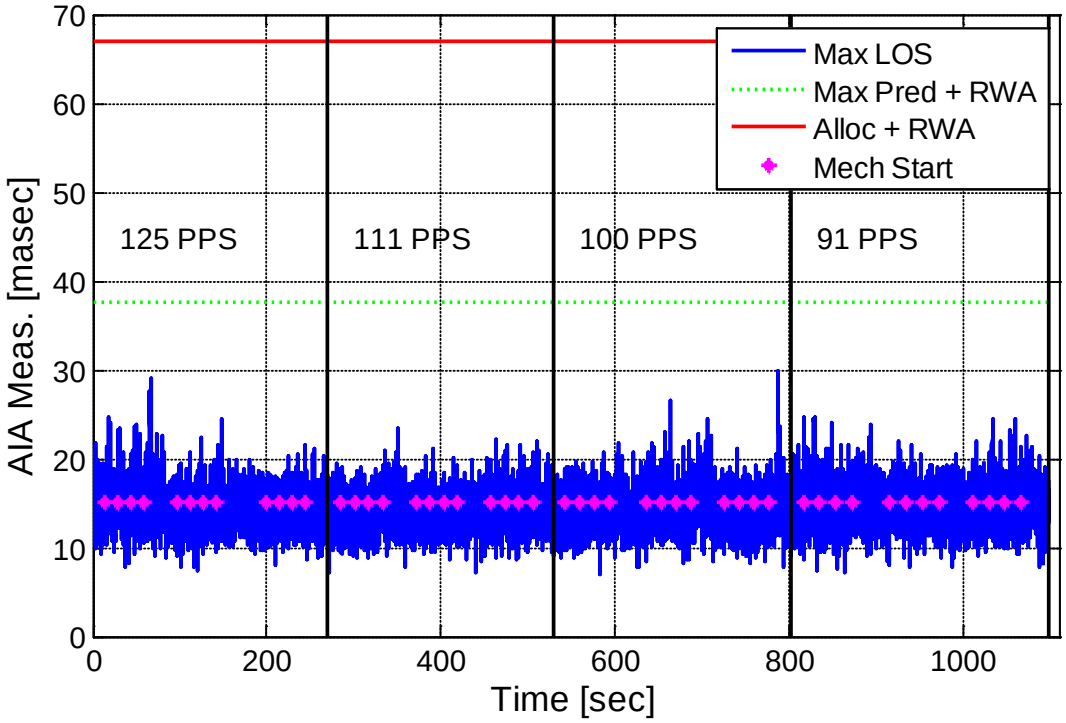

Figure 26 EVE Jitter Test: AIA LOS Error

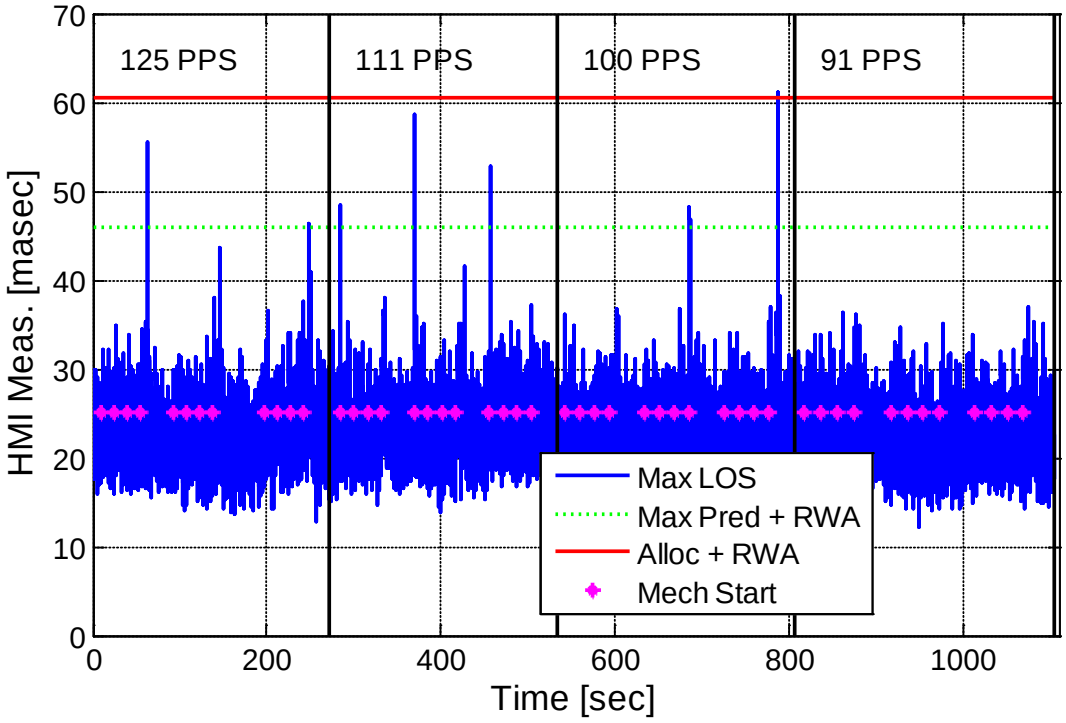

Figure 27 EVE Jitter Test: HMI LOS Error

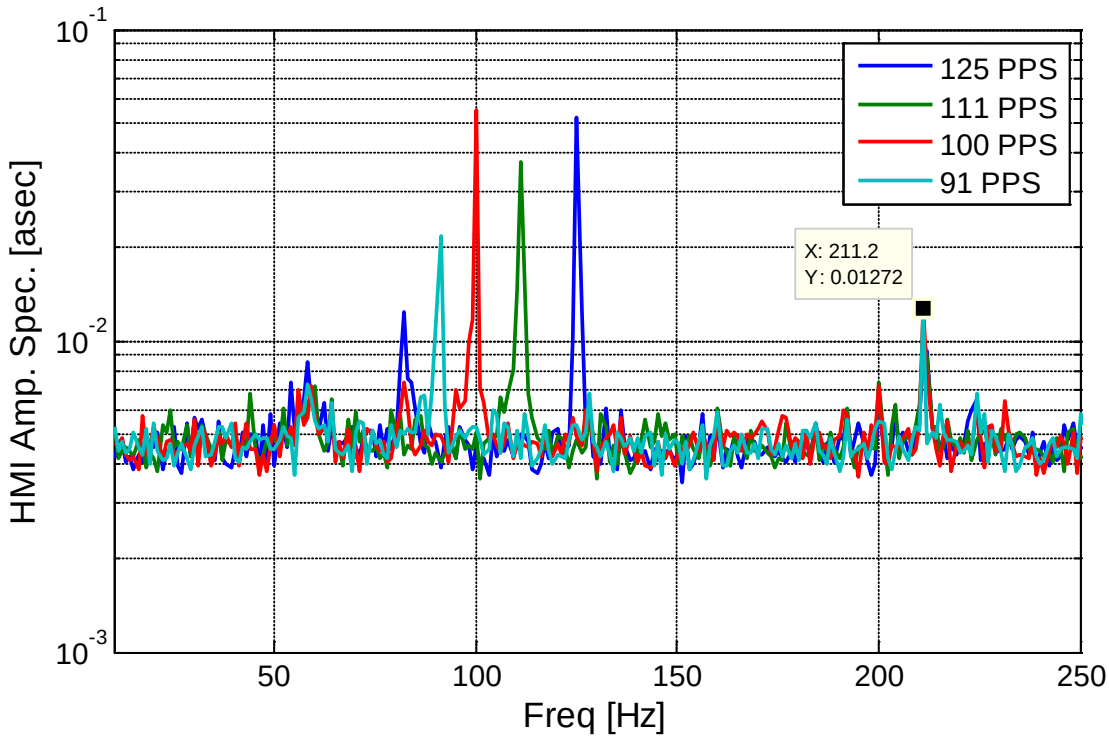

Figure 28 HMI amplitude spectrum during EVE Jitter Test

D. Summary and Jitter Mitigation Applied

The EVE jitter tests demonstrated that a lower EVE step rate (91 PPS) introduces less jitter than the nominal step rate (125 PPS). However, the EVE FW-induced jitter operating at the nominal rate was acceptable to all instruments and met its jitter allocations. Additionally, since the FW environmental and functional tests were performed at the nominal step rate, the SDO team decided to maintain the FW step rate and avoided using a new step rate with fewer ground tests.

VI. AIA Jitter Test

The AIA instrument on board SDO consists of four telescopes. Figure 29 shows their locations and orientations with respect to the spacecraft and the reference coordinate system.

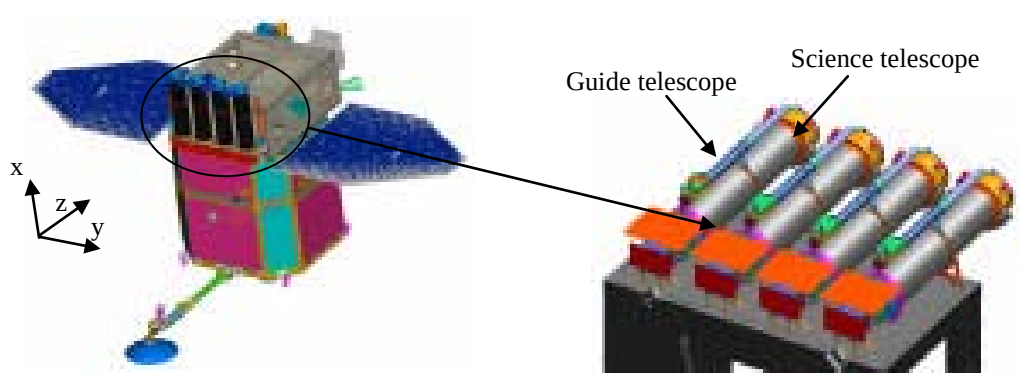

Figure 29 SDO and AIA telescope locations

Each AIA telescope is consisted of 3 different moving mechanisms: a filter wheel (FW), a shutter, and an aperture selector (AS) mechanism. Moving components in these mechanisms are rotating circular disks with various sizes, shape, mass, and inertia. These disks are driven by brushless DC motors, with speed control based on given commutation steps per revolution. The mechanism commutations frequencies are summarized below:

Mechanism	Filter Wheel	Shutter	Aperture Selector
Commutation Frequency	71 Hz	60 Hz	142 Hz

The AIA FWs have the largest moving parts among the three AIA mechanisms. Each FW has 5 positions with move time of one second between adjacent positions. Although operated at relatively low speed of about 0.22 Hz spin rate, the commutation frequency of the AIA FW was set at ~71 Hz which can interact with higher frequency observatory modes. In addition, the AIA FW induced disturbance has start and stop peaks 20 times larger than those produced by the other AIA mechanisms. Based on the pre-launch predictions, the AIA FW induced disturbance was well within its jitter allocation for the HMI LOS. However, larger AIA LOS jitter could be generated if one or more actual observatory modes coincide with the AIA FW commutation frequency. The SDO team designed the AIA jitter test to verify that the FW-induced jitter is acceptable to all instruments as predicted by pre-flight jitter analysis. This knowledge would assist the AIA team in designing their observation sequences to minimize the effects of AIA FW disturbances.

A. Pre-launch Analysis

The AIA FW analysis was performed similarly to the EVE FW analysis. One of the AIA FWs induced vibration disturbances were measured at Lockheed Martin. The test set-up is shown in Figure 30 with the spin torque test data shown in Figure 31. Unlike the EVE FW disturbances, the most noticeable features in the AIA FW disturbance test data are the large amplitudes corresponding to the torque pulses required to start and stop the rotating mechanism. The sinusoidal signature from the commutation steps can also be seen in the measurement data and is most prominently observed over the coasting periods when the FW is essentially at its constant spin rate. The amplitude spectrum plotted on the bottom of Figure 31 illustrates the largest AIA FW disturbance during the coasting period is close to the commutation frequency.

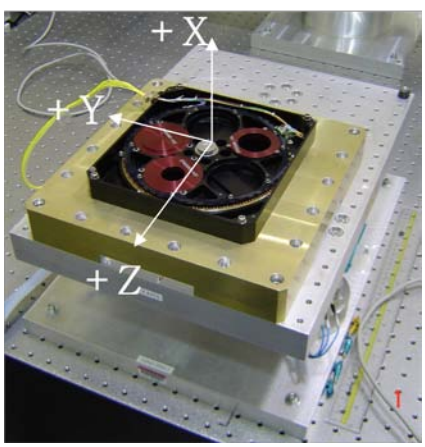

Figure 30 AIA filter wheel test set-up

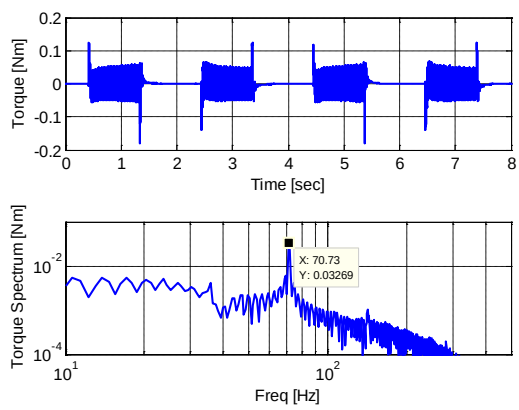

Figure 31 (top) AIA spin torque data (bottom) Amplitude spectrum of torque data

The 3-axis AIA FW measured forces and torques were applied directly to the integrated dynamic model to predict the AIA and HMI LOS motion. Two time simulation scenarios were used for the analysis. The first scenario is the "nominal case" where the mechanisms follow the standard synoptic sequence as described in the next section. The second operational scenario is the "worst case" where three of the four AIA filter wheels are moving at the same time while the telescope without a filter wheel movement takes images. A frequency sensitivity analysis was also performed to vary the input disturbance frequencies by a factor of +/- 10% to account for model frequency uncertainty. In Table 5 the largest LOS jitter from the sensitivity results is reported. The LOS jitter lower bound is given by the largest "nominal case" result, and the higher bound is the largest "worst case" result.

Table 5 Range of Pre-launch AIA FW Induced Jitter From Sensitivity Analysis

	Prediction	Allocation with 100% margin	Allocation
AIA LOS (masec)	63.9 - 94.9	42	84
HMI LOS (masec)	17.7 – 27.8	27.8	55.6

The largest "worst case" AIA LOS prediction exceeds the jitter allocation. Further investigation on the results show that the motor commutation disturbance has a frequency close to several observatory structural modes and can introduce large excitations for the AIA instrument. The situation is exacerbated when three of the wheels move at the same time (i.e. "worst case" operation). It should be emphasized that the jitter performance during the "nominal case" operation meets all jitter allocations. Since three out of four AIA FWs moving simultaneously is an infrequent event, and since the HMI LOS jitter allocation is met, not satisfying the AIA LOS jitter allocation during the "worst case" scenario was determined a minor impact on the AIA science objective. If the AIA FW commutation frequency does indeed excite AIA structural modes, this effect can be detected on orbit. The AIA team could consider redesigning their observing sequences to minimize the AIA FW-induced jitter.

B. Jitter Test Descriptions

During the AIA jitter tests, the AIA team commanded their synoptic observation sequence where FWs, shutters, and aperture selector (AS) moved in a prescribed profile in a 10-sec window. The movement profile is described in detail in Table 6. In normal operations, the AIA FWs rotated back and forth between a couple of positions. After running the synoptic sequence to characterize the jitter response for the default observing sequence, the AIA team commanded each FW sequentially to move back and forth (Table 7) in order to individually measure the jitter associated with the starting and stopping of the FWs.

Both HMI and AIA provided diagnostic data to measure jitter performance, similar to other jitter tests. All the commands to AIA and HMI to turn on data collection, stop data collection, and download the data were sent from the SDO Mission Operations Center. After turning on the instrument diagnostic data collection, the AIA team sent a command to start their synoptic sequence and repeat this sequence six times. Then, a command was sent to start the FW jitter test sequence which was also repeated six times. During the AIA jitter test, the HMI instrument ISS loop was closed, the wheels were kept at low speeds (<300 RPM), and the HGA gimbals and EVE FWs were fixed to isolate jitter induced by the AIA mechanisms.

Table 6 AIA Synoptic Sequence timeline

			AIA Telescope			
start	*time required*	*stop*	1	2	3	4
00:00.0	0:00:10	00:10.0	Start Instrument Diagnostic Data			
0:00:10	0:00:10	00:20.0	Start AIA Jitter Test Sequence			
00:20.0	00:01.0	00:21.0	FW move		FW move	
00:21.0	00:02.0	00:23.0	Idle		Idle	
00:23.0	00:02.0	00:25.0	Shutter exposure		Shutter exposure	
00:22.5	00:01.0	00:23.5		FW + AS move		FW move
00:23.5	00:02.0	00:25.5		Shutter set-up		Shutter set-up
00:25.5	00:02.0	00:27.5		Shutter exposure		Shutter exposure

00:25.0	00:01.0	00:26.0	FW move		FW move	
00:26.0	00:02.0	00:28.0	Idle		Idle	
00:28.0	00:02.0	00:30.0	Shutter exposure		Shutter exposure	
00:27.5	00:01.0	00:28.5		FW + AS move		FW move
00:28.5	00:02.0	00:30.5		Shutter set-up		Shutter set-up
00:30.5	00:02.0	00:32.5		Shutter exposure		Shutter exposure
00:32.5	00:12.5	00:45.0	IDLE			

Table 7 AIA FW jitter test timeline

			AIA Telescope			
start	*time required*	*stop*	1	2	3	4
00:45.0	00:01.0	00:46.0	FW Move			
00:46.0	00:05.0	00:51.0	IDLE			
00:51.0	00:01.0	00:52.0	FW Move			
00:52.0	00:05.0	00:57.0	IDLE			
00:57.0	00:01.0	00:58.0		FW move		
00:58.0	00:05.0	01:03.0	IDLE			
01:03.0	00:01.0	01:04.0		FW move		
01:04.0	00:05.0	01:09.0	IDLE			
01:09.0	00:01.0	01:10.0			FW Move	
01:10.0	00:05.0	01:15.0	IDLE			
01:15.0	00:01.0	01:16.0			FW Move	
01:16.0	00:05.0	01:21.0	IDLE			
01:21.0	00:01.0	01:22.0				FW move
01:22.0	00:05.0	01:27.0	IDLE			
01:27.0	00:01.0	01:28.0				FW move
01:28.0	00:12.0	01:40.0	IDLE			

C. Jitter Measurements

The maximum AIA LOS jitter (over four telescopes and two LOS axes) during the AIA jitter test is shown in Figure 32. The left portion of the figure illustrates the measured jitter during the AIA Synoptic Sequence where two AIA FWs move at the same time. The FW-alone jitter measurements are plotted in the right portion of the figure, where six sets of FW movements can be easily seen. After two sets of the FW sequence were performed, the sensor data was downloaded to the ground before starting another two sets of tests. In between two sets of the FW sequence, a pause of 20 sec was supposed to be inserted to separate the test sets. However, due to a programming error in the test setup, the first pulse of the second set was commanded before the 20-sec break takes place. Therefore, there are 9 peaks in the first and 7 peaks in the second FW sequence set, corresponding to when each AIA FW started/stopped. The line width makes the start and stop pulses indistinguishable. Interestingly, the FW in

AIA telescope #1 generated much lower jitter than the other three filter wheels. This result could indicate that AIA FW#1 may be better balanced than the other FWs.

More importantly, Figure 32 shows the pre-launch prediction plus largest wheel-induced jitter (under 300 RPM) envelops the maximum AIA LOS error (blue line) for all step rates tested. The AIA mechanism-induced jitter during the standard synoptic sequence also meets the jitter allocation (red line) with significant margin. Although the "worst case" operational scenario, where three FWs move at the same time, was not exercised during jitter testing, the results from the synoptic sequence with two FWs moving at the same time provide some confidence that the AIA jitter allocation can be met in the "worst case" scenario. From the on-orbit test data, the team determined the likelihood of the AIA FW commutation frequency exciting a major observatory mode to be low.

Figure 33 illustrates the maximum HMI LOS jitter (over the tip/tilt axes) measured during the AIA jitter test. The HMI LOS measurements show that it is relatively insensitive to the AIA mechanism movements, including the FW. It is difficult to distinguish between AIA FW-induced and reaction wheel-induced jitter in the HMI LOS measurements. The HMI LOS jitter allocation is met in this case with the pre-launch prediction bounding the on-orbit HMI LOS errors.

Since AIA LOS measurements showed greater responses to the AIA mechanism-induced disturbances, the spectral analysis was performed on the AIA LOS sensor, instead of the HMI LOS data as for previous jitter test results. The AIA Telescope 1 sensor measurements, sampled at 256 Hz, were used for the spectral analysis. The amplitude spectra for the synoptic sequence and three sets of two FW jitter sequences are shown in Figure 34. The LOS jitter associated with the FW commutation frequency at ~71 Hz has the largest disturbance amplitude for both the synoptic sequence (blue line) and FW jitter sequences as expected. The shutter commutation frequency at ~60 Hz is also present in the spectrum plot for the synoptic sequence. The aperture selector's commutation frequency is 140 Hz which is slightly above the sensor Nyquist frequency and not observable at the aliased frequency (20 Hz). There is an ~81 Hz disturbance appearing for all AIA test sequences. This disturbance is likely to be the aliased 210 Hz disturbance with unidentified source that is present in all jitter test data.

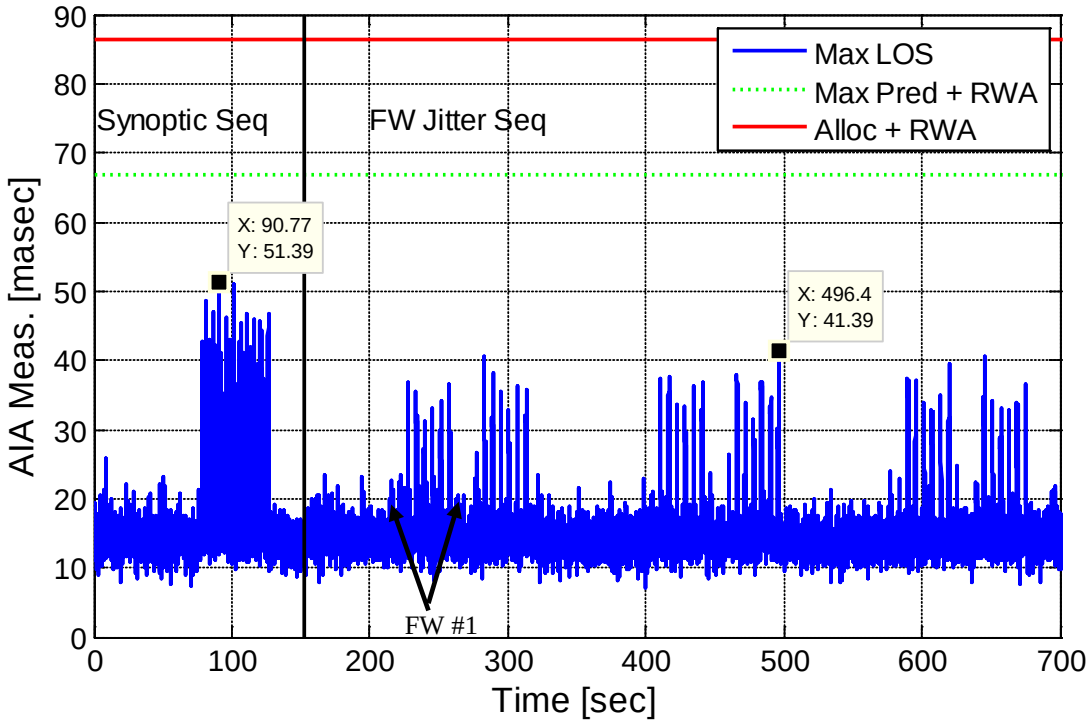

Figure 32 Maximum AIA LOS during AIA Jitter Test

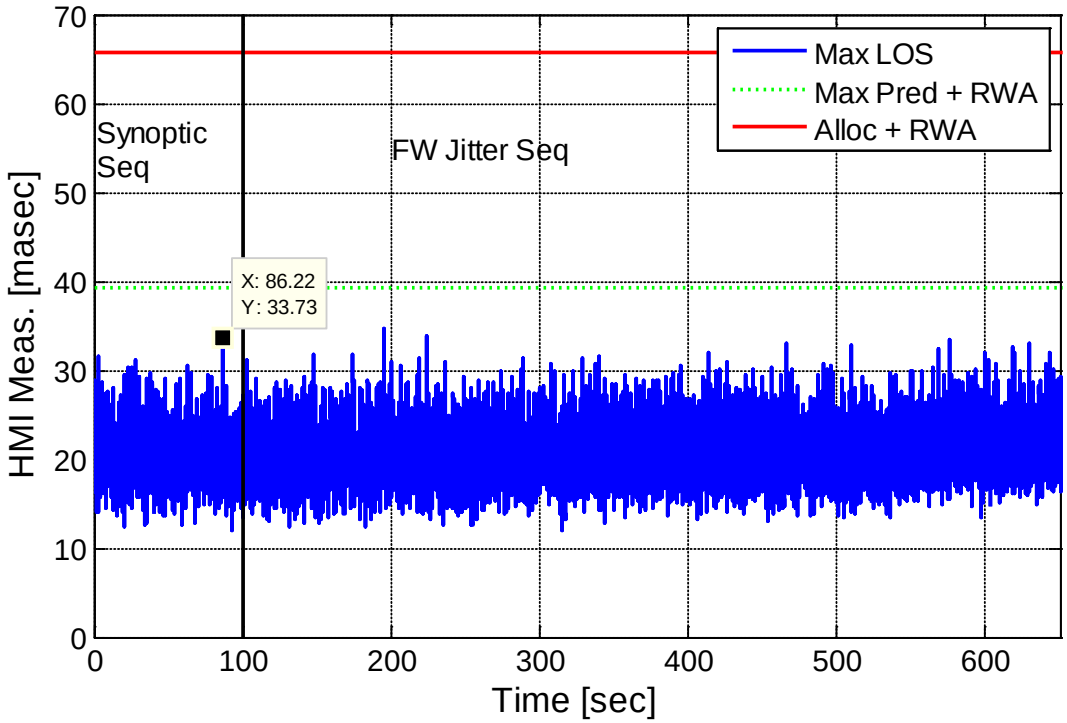

Figure 33 Maximum HMI LOS during AIA Jitter Test

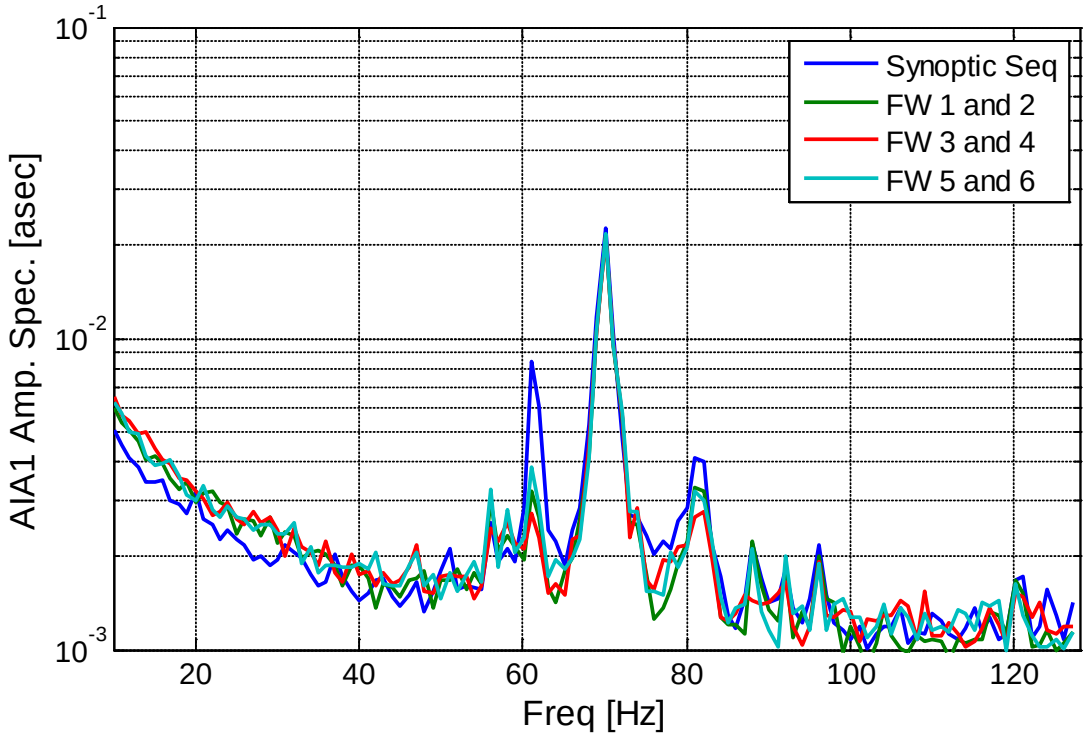

Figure 34 AIA Telescope #1 amplitude spectrum for AIA Jitter Test

D. Summary and Jitter Mitigation Applied

The on-orbit jitter measurements show AIA mechanism induced disturbances are acceptable to both AIA and HMI. The FW commutation frequency disturbance does not cause AIA LOS to violate jitter requirement. The Synoptic sequence test data also shows that the AIA jitter allocation is met with a good margin. Therefore, no additional mitigation plan was required to reduce AIA FW disturbances.

VII. Summary and Conclusion

The largest LOS measurements with no HGA jitter mitigations applied (and therefore the largest gimbal rate is limited to 43 deg/hr) and instrument jitter allocations are summarized in Table 8. In this table, the reaction wheel speed limit is set to 850 RPM, and the EVE step rate is the nominal rate of 125 PPS. The HMI instrument mechanism induced-jitter was not measured during the on-orbit jitter test, since its impact was determined to be small. The LOS jitter due to the HMI mechanism is assumed to be the same as its jitter allocation as a worst case bound. There are other minor jitter contributing sources such as the wheel torque noise and sensor quantization noise that are also included in this table. These other jitter sources were present during the reaction wheel jitter test, and therefore, the LOS errors induced by them were included in the largest reaction wheel LOS measurements. If SDO were to operate with no HGA mitigation method, the total HMI LOS jitter (root-sum-squared of all measured jitter contributions) would violate the HMI jitter requirement. As a result, the HGA stagger step and the HMI NSR flag were used to reduce HGA-induced jitter.

Table 9 summarizes the largest jitter measurements with HGA jitter mitigation strategies implemented. Using these strategies, the HGA gimbals were allowed to have a maximum step rate of 140 deg/hr. The increased gimbal rate causes the AIA LOS HGA jitter to increase above its allocation, but since moving the HGA at this maximum is an infrequent occurrence, AIA can still meet its jitter requirement of 95% data collection continuity. Activating the HMI NSR flag effectively reduces the HMI HGA jitter by a factor of 3 based on analysis and on-orbit test data[4]. This mitigation method allows the HMI to meet its jitter requirement. It should be noted that if only the HMI NSR flag is used, the HGA pointing algorithm should not reject any requests under the current operational condition[4]. However, if the AIA NSR is also used, the AIA requests will be made at different times than the HMI NSR, accumulating too many requested pauses in HGA tracking. In this case, some of the AIA requests would be rejected in order to maintain lock on the ground station. To simplify the operational scenario, the SDO team decided to turn only the HMI NSR flag on and leave the AIA NSR flag off.

Table 8 Maximum LOS measurements (with no HGA mitigation) and instrument allocations

Jitter Source	Max AIA LOS Meas. (masec)	AIA Alloc. (masec)	Max HMI LOS Meas. (masec)	HMI Alloc. (masec)
RWA (<=850 RPM)	35.4	70.0	36.5	62.6
HGA (<= 43 deg/hr)	125.3	106.0	165.8	94.0
EVE (125 PPS)	21.1	64.0	43.1	49.4
AIA	47.3	84.0	18.8	55.6
HMI	28.0	28.0	33.4	33.4
Other sources	in RWA Meas.	28.8	in RWA Meas.	14.1
RSS Total	142.9	170.0	179.3	140.0

Table 9 Maximum LOS measurements (with HGA mitigation) and instrument allocations

Jitter Source	Max AIA LOS Meas. (masec)	AIA Alloc. (masec)	Max HMI LOS Meas. (masec)	HMI Alloc. (masec)
RWA (<850 RPM)	35.4	70.0	36.5	62.6
HGA (<= 140 deg/hr)	130.7	106.0	69.1	94.0
EVE (125 PPS)	21.1	64.0	43.1	49.4
AIA	47.3	84.0	18.8	55.6
HMI	28.0	28.0	33.4	33.4
Other	In RWA Meas.	28.8	In RWA Meas.	14.1
RSS Total	147.7	170.0	97.1	140.0

The four main objectives of the jitter tests were achieved after the completion of the jitter test:

1. The acceptable reaction wheel operational speed range during Science Mode was extended to +/-850 RPM from +/-412 RPM.
2. The HGA jitter mitigation methods included implementing the stagger stepping option and the HMI NSR flag.
3. The EVE FW step rate remained at the nominal 125 PPS.
4. The AIA instrument mechanisms generated acceptable disturbances to AIA and HMI. The AIA team was not required to redesign the instrument's observation sequence.

Some of the important lessons learned from managing and analyzing SDO jitter are summarized below:

- For jitter sensitive missions (sub-arcsecond level requirements):
  - Early jitter assessment to identify what protective steps are necessary.
  - Instrument mechanisms: ability to vary step frequency or commutation frequency on-orbit to avoid exciting structural modes
  - Reaction wheel: include wheel structural amplifications in disturbance model especially if wheels are operated at low wheel speeds to minimize jitter. Evaluate the effect of the broadband noise signature.
  - HGA: consider micro-stepping and implement pointing algorithm to allow random and stagger stepping
  - Provide for coordination between telescope and mechanism operations
  - Every disturbance source should be measured as early as possible
- High modal density can create amplification that greatly exceeds typical back-of-the-envelope estimates
  - Typical estimate is that dynamic amplification Q=500 (for a 0.1% damped structure) above rigid body motion
  - SDO structure exhibited amplification of 10^3-10^4 in 30-80 Hz region above rigid body motion
- Jitter is a system level problem that cannot be treated adequately at the component level
  - Allocate separate budget for jitter modeling and analysis work
  - Jitter requirement should be set at the detector (using integrated model) and not at instrument mounting interface
  - Plan model verification, validation, and calibration work early
- Requirements on model fidelity are needed on FEM to address jitter
- On-orbit jitter test and mitigation strategies should be included in the overall jitter management program

The SDO project took the extraordinary step to measure jitter on orbit. This unique on-orbit test data has provided, and will continue to provide, invaluable engineering data for validating jitter model and analysis approaches.

Acknowledgments

The authors would like to remember Dr. William Haile for his instrument mechanism jitter analysis, test support, and dynamics insights on the SDO jitter team. The authors would also like to thank Seth Shulman and Peter Kutt for their support and participation during the SDO on-orbit jitter tests, and Peter Mule for providing and integrating observatory structural models.

Reference

[1]Kuo-Chia (Alice) Liu, Thomas Kenney, Peiman Maghami, Pete Mule, Carl Blaurock, and William B Haile. Jitter Test Program and On-Orbit Mitigation Strategies for Solar Dynamics Observatory. International Symposium on Space Flight Dynamics, 2007.

[2]Carl Blaurock, Kuo-Chia Liu, and Peter Mule. Solar Dynamics Observatory (SDO) HGAS Induced Jitter. 49th AIAA/ASME/ASCE/AHS/ASC Structures, Structural Dynamics, and Materials Conference, 2008, AIAA 2008-1951.

[3]Kuo-Chia Liu and Peiman Maghami, and Carl Blaurock. Reaction Wheel Disturbance Modeling, Jitter Analysis, and Validation Tests for Solar Dynamics Observatory. AIAA Guidance, Navigation and Control Conference and Exhibit, 18 - 21 August 2008, Honolulu, Hawaii. AIAA 2008-7232.

[4]Kristin L. Bourkland, Kuo-Chia (Alice) Liu. Verification of the Solar Dynamics Observatory High Gain Antenna Pointing Algorithm Using Flight Data. AIAA Guidance, Navigation, and Control Conference, 8-11 August 2011, Portland, Oregon.

[5]Haile, William, "EVE Filter Wheel Analysis," NASA Goddard Space Flight Center, Rept. 464-ACS-RPT-0198, Greenbelt, MD, Oct. 2007.

[6]W. Morgenstern, K. Bourkland, et al. Solar Dynamics Observatory Guidance, Navigation, and Control System Overview. AIAA Guidance, Navigation, and Control Conference, 8-11 August 2011, Portland, Oregon.